IEEE Access
Multidisciplinary ⋮ Rapid Review ⋮ Open Access Journal

Received March 28, 2021, accepted April 8, 2021, date of publication April 14, 2021, date of current version April 27, 2021.

*Digital Object Identifier 10.1109/ACCESS.2021.3073117*

# Transient Energy of an Individual Machine PART II: Potential Energy Surface

**SONGYAN WANG[1], JILAI YU[1], AOIFE M. FOLEY[2], (Senior Member, IEEE), AND WEI ZHANG[1], (Senior Member, IEEE)**

[1]Department of Electrical Engineering, Harbin Institute of Technology, Harbin 150006, China
[2]School of Mechanical and Aerospace Engineering, Queen's University Belfast, Belfast BT7 1NN, U.K.

Corresponding author: Songyan Wang (wangsongyan@163.com)

**ABSTRACT** In this second paper, the individual-machine potential energy surface is established. The constant-$\theta_i$ angle surface of the machine is found in the angle space. Because the individual-machine potential energy is strictly zero in this angle surface, the constant-$\theta_i$ angle surface has a significant effect on the shape of the individual-machine potential energy surface. That is, the individual-machine potential energy surface is separated by a flat land, and mountains and valleys are located on either side of this flat land. In addition, a zero-$f_i$ angle surface also exists in the individual-machine potential energy surface. The individual-machine potential energy reaches a minimum or maximum at the surface. Using a scissor angle surface, the individual machine potential energy boundary that reflects the maximum individual-machine potential energy is obtained through the cut of the zero-$f_i$ angle surface. The machine becomes unstable after the system trajectory goes through the individual machine potential energy boundary. In the end, key concepts and distinctive phenomena in the individual-machine studies are fully explained using the concept of individual-machine potential energy surface.

**INDEX TERMS** Transient stability, transient energy, individual machine, potential energy surface.

## NOMENCLATURE

| | |
|---|---|
| RM | Reference machine |
| DLP | Dynamic liberation point |
| DSP | Dynamic stationary point |
| EAC | Equal area criterion |
| LUM | Leading unstable machine |
| MOD | Mode of disturbance |
| MPP | Maximum potential energy point |
| PEB | Potential energy boundary |
| PES | Potential energy surface |
| SEP | Stable equilibrium point |
| TSA | Transient stability assessment |
| UEP | Unstable equilibrium point |
| GPES | Global PES |
| GPEB | Global PEB |
| IMKE | Individual-machine kinetic energy |
| IMPE | Individual-machine potential energy |
| IMTE | Individual-machine transient energy |
| IMTR | Individual-machine trajectory |
| IMPP | Individual-machine MPP |
| LOSP | Loss-of-synchronism point |
| RUEP | Relevant UEP |
| SSAS | Second scissor angle surface |
| IMEAC | Individual machine EAC |
| IMPEB | Individual-machine PEB |
| IMPES | Individual-machine PES |

The associate editor coordinating the review of this manuscript and approving it for publication was Xiaorong Xie.

## I. INTRODUCTION

### A. LITERATURE REVIEW

Potential energy surface (PES) is proposed to visually describe the variance of the transient energy along different system trajectories. In classic transient energy analysis, the multimachine stability problem is visualized as an energy ball rolling in the PES. The ball escapes from the potential energy boundary (PEB) when it receives just enough energy from the fault condition to reach the saddle point and pass through it. During this transient process, conversion between kinetic energy and potential energy would occur along the track of the energy ball. Motivated by the concept of PES, Kakimoto [1], [2] replaced the actual system trajectory with a fictional sustained fault trajectory to obtain the critical

potential energy that occurs in PEB. Athay [3] observed that the critical transient energy of the system is close to the energy at the relevant unstable equilibrium point (RUEP) that lies in PEB. In brief, early transient energy methods are essentially established based on the concept of PES.

The sustained fault method and the RUEP method are defined using the global transient energy, i.e., the Superimposed transient energy of all machines in the system. Therefore, the two methods are naturally formed based on the ''global'' PES (GPES). In modern transient stability assessment (TSA), the concept of GPES completely fades in group equivalent methods because the entire multimachine system is depicted in an equivalent two-machine form. Notably, compared with the fading of the GPES, the early individual-machine analysts conjectured that an individual-machine PES (IMPES) might also exist in TSA. Michel and Vittal attempted to split the GPES into individual-machine slices. These individual-machine analysts conjectured that ''if the fault is kept long enough for one machine (or more) to become critically unstable, the potential energy of the critical machine goes through a maximum before instability occurs'' [4], [5]. Later, Stanton [6] conjectured that the maximal potential energy of the individual machine would specify an individual-machine PEB (IMPEB) in the angle space. Ando [7] also discovered that IMPEB could be used to characterize the stability of the system.

Although hypotheses about IMPES were already given in history, this research was at a standstill for decades because of the imperfections of early individual-machine studies. Recent advances show that the individual machine equal area criterion (IMEAC) method may be promising in TSA [8]–[10], which further inspires the exploration of IMPES. Before the studies of this novel concept are conducted, the following issues are always questioned by global analysts:

(i) What are the distinctive characteristics of IMPES?

(ii) What is the mathematical expression of IMPEB?

The exploration of the mechanism of IMPES may theoretically validate the effectiveness of the IMEAC method [8]–[10]. Furthermore, the establishment of IMPES may lead to systematic redefinitions of the transient energy in a genuine individual-machine manner. This research may help readers gain deep insights into the physical nature of the individual-machine approach.

### B. SCOPE AND CONTRIBUTION OF THE PAPER

Following the individual-machine potential energy (IMPE) as defined in the first paper [11], this paper systematically establishes fundamental theories of the IMPES. It is found that a constant-$\theta_i$ angle surface exists in the IMPES. This angle surface is distinctive because the IMPE of Machine $i$ is strictly zero in it. Meanwhile, the IMPE around the constant-$\theta_i$ angle surface is rather low; thus, the IMPES is separated by a ''flat land'' with very low IMPE. Mountains and valleys are located on either side of this flat land. Furthermore, detailed modeling of the IMPES is obtained using IMPE along rays. In addition, a zero-$f_i$ angle surface also exists in the IMPES. The IMPE might reach extrema (maximum or minimum) at the zero-$f_i$ angle surface. To obtain the IMPEB where the IMPE reaches a maximum, a scissor angle surface is developed to cut the IMPEB from the zero-$f_i$ angle surface. The machine becomes unstable after the system trajectory goes through the IMPEB. In the end, key concepts and distinctive phenomena in the individual-machine studies are explained using the concept of IMPES.

The contributions of this paper are summarized as follows:

(i) This is the first time the IMPES is proposed in the history of individual-machine studies. Individual-machine transient characteristics are depicted effectively through IMPES.

(ii) Distinctive characteristics of IMPEB are analyzed. The instability of a critical machine is precisely characterized through IMPEB.

(iii) Distinctive phenomena in the individual-machine studies are theoretically explained using IMPEB. This approach validates the effectiveness of the recently developed IMEAC method.

The remainder of the paper is organized as follows. In Section II, the constant-$\theta_i$ angle surface is proposed. In Section III, the IMPES is modeled using rays. In Section IV, the IMPEB of each machine is formed by using zero-$f_i$ angle surface and the scissor angle surface. In Section V, case studies are provided to demonstrate the concept of IMPES and IMPEB. In Section VI, concepts and distinctive phenomena in the IMEAC method are theoretically explained using IMPES. Conclusions and a discussion are provided in Section VII.

In this paper, it should be clarified that IMPES is a surface that is formed by both IMPE and angles. Comparatively, IMPEB, constant-$\theta_i$ angle surface, zero-$f_i$ angle surface and scissor angle surface are genuine angle surfaces that are defined only by the angles of the machines in the system.

## II. CONSTANT-THETA ANGLE SURFACE

### A. RULER IMTR

In this section, we first focus on the mechanism of the IMPES of only one machine in a multi-machine system. After that, in Section III it will be extended to the case of multiple IMPESs, because each machine in a multi-machine system corresponds to its unique IMPES.

Following the analysis in the first paper [11], the IMPE of Machine $i$ is denoted as

$$V_{PEi} = \int_{\theta_i^s}^{\theta_i} \left[ -f_i^{(PF)}(\boldsymbol{\theta}) \right] d\theta_i \tag{1}$$

From Eq. (1), the energy reference point of $V_{PEi}$ is set as $\theta_i^s$. If the postfault structure of the power system is fixed, $V_{PEi}$ will vary with the changes of the system trajectories because it is completely decided by the system trajectory ($\boldsymbol{\theta}$).

If we observe an actual multimachine system trajectory, the original point of the trajectory is a stable equilibrium point (SEP), and thus the original point of each individual-machine trajectory (IMTR) is $\theta_i^s$. We assume that a very distinctive IMTR is given. The angle of this IMTR remains constant

along the time horizon. This distinctive IMTR is denoted as

$$\theta_i^t = \theta_i^s \tag{2}$$

From Eq. (2), this IMTR of Machine $i$ is "horizontal" in the $t$-$\theta$ space. This IMTR is a fictional ideal IMTR because it *cannot* be obtained from actual simulations.

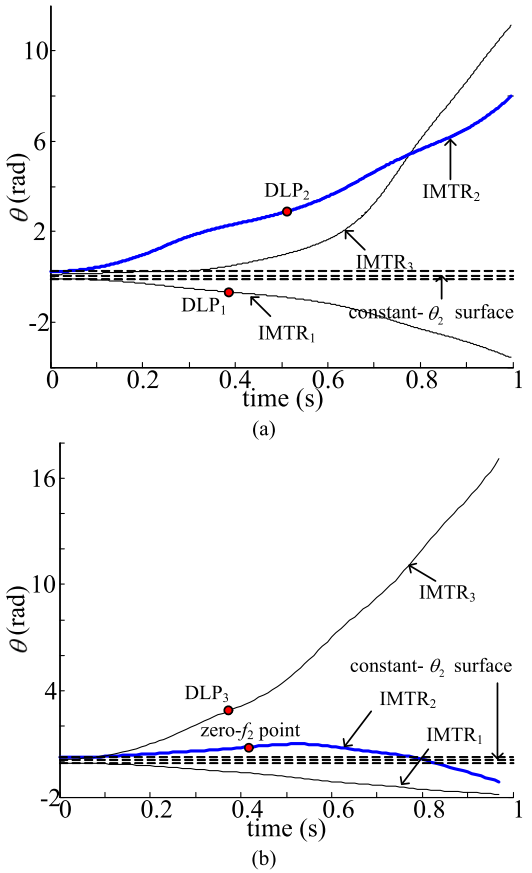


**FIGURE 1.** Demonstration of ruler IMTR. (a) Case-1 and (b) Case-2.

This fictional IMTR can be set as the "ruler" to measure the fluctuation of the IMTR of Machine $i$. In this paper, it is named the "ruler IMTR". Two cases are given below, as in Fig. 1. Case-1 is [TS-4, bus-2, 0.25 s]. Case-2 is [TS-4, bus-3, 030 s]. We only focus on the transient behavior of Machine 2 as an representation. In Case-1, the actual $IMTR_2$ separates from the ruler $IMTR_2$, and Machine 2 is an unstable critical machine. Comparatively, in Case-2, the actual $IMTR_2$ is close to the ruler $IMTR_2$, and Machine 2 is a non-critical machine.

### B. RELATIONSHIP BETWEEN IMPE AND RULER IMTR

Following the analysis in Section V as in the first paper [11], in this part, the relationship between IMPE and the actual IMTR will be further explained using the concept of the ruler IMTR.

In a multimachine system with $n$ machines, each machine has its unique corresponding ruler IMTR. Although the ruler IMTR of a machine is fictional, its corresponding IMPE can still be computed. The IMPE of Machine $i$ with ruler $IMTR_i$ is denoted as

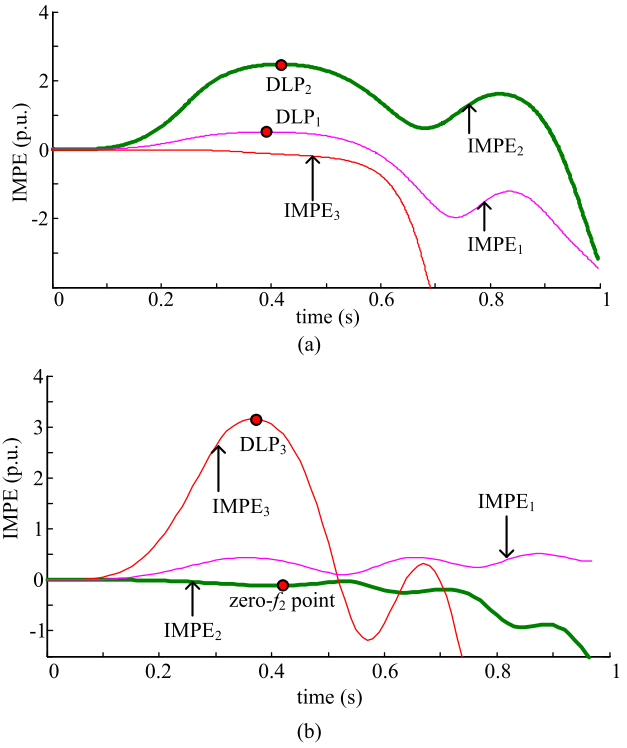


**FIGURE 2.** Variance of $IMPE_2$. (a) Case-1. (b) Case-2.

$$V_{PEi} = \int_{\theta_i^s}^{\theta_i} \left[-f_i^{(PF)}\right] d\theta_i = \int_{\theta_i^s}^{\theta_i} \left[-f_i^{(PF)}\right] d\theta_i^s = 0 \tag{3}$$

Eq. (3) indicates that the $IMPE_i$ along its ruler IMTR is strictly zero. Briefly, the ruler IMTR is not only used as the "ruler" of separation of the actual IMTR but is also used as the "ruler" of the variance of the IMPE along the time horizon. In particular, if the actual IMTR of the machine is always close to its ruler IMTR along the time horizon, the machine is a non-critical machine with slight variance of the IMPE; in contrast, if the actual IMTR of the machine goes far from its ruler IMTR along the time horizon, the machine is a critical machine with severe variance of the IMPE.

The definition of the ruler IMTR is of key importance because it indicates that the variance of the IMPE of the machine can be measured through the separation between the actual IMTR and the ruler IMTR of the machine. A tutorial example of the variance of $IMPE_2$ is shown in Fig. 2.

From Fig. 2, in Case-1, $IMPE_2$ becomes negative infinite with infinite $IMTR_2$ because actual $IMTR_2$ goes far from ruler $IMTR_2$, as in Fig. 1 (a). Comparatively, in Case-2, $IMPE_2$ varies only slightly because the actual $IMTR_2$ is very close to ruler $IMTR_2$, as in Fig. 1 (b).

The analysis above indicates the following

*The variance of the IMPE of the machine strongly correlates to the separation between the actual IMTR and the ruler IMTR of the machine.*

From the analysis above, although the IMPE of a machine is decided by the entire multimachine system trajectory ($f_i(\boldsymbol{\theta})$ is formed by of all machines in the system as in Eq. (1)), the IMPE of the machine is mainly decided by the variance of the IMTR of the machine. Therefore, the key factor that affects the variance of the IMPE of a machine should be the "separation" between the actual IMTR and the fictional ruler IMTR of the machine. The characteristics of the ruler IMTR further validate the analysis in the first paper [11].

### C. DEFINITION OF THE RULER IMTR IN THE ANGLE SPACE

Following the definition of IMPE as Eq. (1), the IMPE of a machine is only depicted by using the system trajectory ($\boldsymbol{\theta}$). In other words, although the actual system trajectory is depicted in the $t$-$\theta$ space, the IMPE is only decided by $\boldsymbol{\theta}$ at each simulation step without using $t$.

We further define the system trajectory in a genuine angle manner. Assume the time horizon is eliminated from the system trajectory. In this way, the system trajectory is redescribed in the multimachine angle space. For a multimachine system with $n$ machines, the angle space in the COI-SYS reference may reach $n$-1 hyper-dimensions because the $\theta_n$ is not independent. Note again that $t$ becomes fade and imaginary in the angle space.

In the angle space, the ruler IMTR of Machine $i$ is redescribed as an "angle surface". The function of this surface is denoted as

$$\theta_i = \theta_i^s \tag{4}$$

In this paper, the angle surface in Eq. (4) is named the "constant-$\theta_i$ angle surface". For a multimachine system, each machine corresponds to its unique constant-$\theta_i$ angle surface. Following Eq. (3), the IMPE$_i$ along each constant-$\theta_i$ angle surface is also strictly zero in the angle space.

The system trajectories of Case-1 and Case-2 in the angle space are shown in Fig. 3. We only observe the transient behavior of Machine 2 for representation.

From Fig. 3, in the angle space, the constant-$\theta_2$ angle surface is depicted as a straight line in this three-machine system. The actual IMTR of a machine that is defined in the $t$-$\theta$ space as in Fig. 1 disappears because $t$ is eliminated. Instead, the separation between the actual IMTR$_i$ and the ruler IMTR$_i$, as analyzed in Fig. 1 is redepicted as the "distance" between the actual system trajectory along the $\theta_i$ axis and the constant-$\theta_i$ angle surface with the elimination of $t$.

Following the relationship between IMPE and IMTR of the machine as analyzed in Section B, detailed analysis about the transient energy behavior of Machine 2 in the angle space is shown below

*Variance of the IMPE$_2$ in the angle space with Case-1*: Since the system trajectory along the $\theta_2$ axis leaves far from the constant-$\theta_2$ angle surface (in this case the actual IMTR$_2$ separates from the ruler IMTR$_2$ in the $t$-$\theta$ space, as in Fig. 1 (a)), IMPE$_2$ first reaches a maximum and then becomes negative infinite along the system trajectory, as in Fig. 2 (a). Machine 2 also becomes an unstable critical machine.

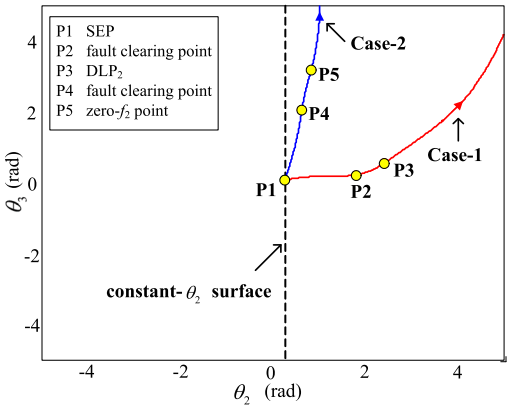


**FIGURE 3.** Constant-$\theta_2$ angle surface.

*Variance of the IMPE$_2$ in the angle space with Case-2*: Comparatively, since the system trajectory along the $\theta_2$ axis is close to the constant-$\theta_2$ angle surface (in this case the actual IMTR$_2$ is close to the ruler IMTR$_2$ in the $t$-$\theta$ space, as in Fig. 1 (b)), IMPE$_2$ varies slightly along the system trajectory, as in Fig. 2 (b). Machine 2 becomes a non-critical machine.

From analysis above, following the relationship between the IMTR and IMPE as analyzed in Section B, in the angle space, the relationship between the system trajectory and the IMPE is summarized as follows:

(i) If the system trajectory along the $\theta_i$ axis is close to the constant-$\theta_i$ angle surface, the IMPE$_i$ varies slightly along time horizon. Machine $i$ would be a non-critical machine.

(ii) If the system trajectory along the $\theta_i$ axis leaves far from the constant-$\theta_i$ angle surface with time, the IMPE$_i$ first reaches a maximum and later becomes negative infinite along the time horizon. Machine $i$ would be an unstable critical machine.

(iii) If the system trajectory along the $\theta_i$ axis leaves far from the constant-$\theta_i$ angle surface at first but inflects back later, the IMPE$_i$ is bounded along time horizon. Machine $i$ would be a stable critical machine.

The deductions above fully reflect the variance of the IMPE$_i$ through the relative motion between the actual system trajectory and the constant-$\theta_i$ angle surface in the angle space.

In the following sections, all the analysis about the shape of the IMPES will be transformed into the angle space. It will be validated that the constant-$\theta_i$ angle surface has a significant effect on the shape of the IMPES. In addition, since detailed studies in the $t$-$\theta$ space are already given in Section A, they can be used as the comparisons of the transient analysis in the angle space in the following paper.

## III. THE MODELING OF IMPES

### A. FORMATIONS OF THE IMPES

Based on the analysis in Section II B, assume numerous system trajectories form a "trajectory set" in the angle space. Each system trajectory in this set corresponds to the IMPE of Machine $i$ along it. Next, one naturally deduces that these

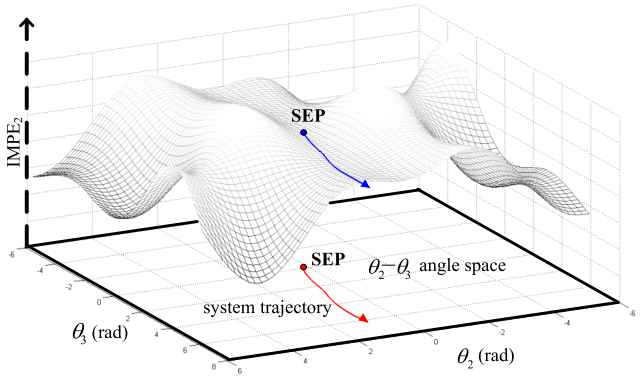


**FIGURE 4.** Formations of IMPES$_2$.

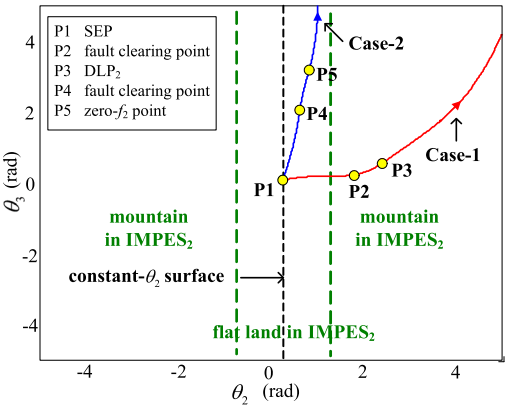


**FIGURE 5.** Shape of the IMPES$_2$ using simplified IMPES.

IMPEs of Machine *i* under different system trajectories may form a "potential energy surface" of a machine.

In this paper, we name this surface the "individual-machine potential energy surface" (IMPES). Briefly, the IMPES is seen as the extension of the angle space with one more dimension, i.e., the IMPE along the "altitude". A demonstration of the formation of IMPES is shown in Fig. 4. The actual system trajectory in the figure corresponds to Case-2. In this case, we still focus on the IMPES of Machine 2 for representation.

From Fig. 4, assume the IMPE is an energy ball that rolls on the energy "basin", i.e., IMPES. The ball has a "track" associated with its motion. The projection of the track on the angle space is only the actual system trajectory ($n$-1 dimension), while the projection of the track on the altitude reflects the variance of IMPE along the actual system trajectory. The SEP represents the zero-altitude point in the IMPES (IMPE at SEP is zero), and it is also the point where the energy ball originates. The energy ball might escape from the basin, depending on the energy it receives from fault conditions. The motion of the energy ball in the IMPES may visually reflect the variance of the IMPE of the machine along the system trajectory.

### B. EXPLORATION OF THE IMPES USING CONSTANT-THETA ANGLE SURFACE

The effectiveness of the IMPES leads to the emergence of the first question: what is the shape of the IMPES?

In this paper, we state the following

*The constant-$\theta_i$ angle surface has a significant effect on the shape of the IMPES of Machine i.*

In the two-dimensional angle space, affected by the constant-$\theta_i$ angle surface, the IMPES is visually formed by a flat land, and mountains and valleys on either side of the flat land. A detailed analysis is given below.

#### 1) FLAT LAND

Following the analysis in Section II C, the IMPE$_i$ along the constant-$\theta_i$ angle surface is strictly zero. We proceed a further step. In the angle space, for a certain system trajectory along the $\theta_i$ axis that is close to the constant-$\theta_i$ angle surface, it is certain that the IMPE$_i$ along this system trajectory varies very slightly. Under this circumstance, a large area which is close to the constant-$\theta_i$ angle surface should be quite flat.

The first characteristic of the IMPES is given as follows.

*A flat land exists in each IMPES.*

Briefly, the flat land in each IMPES is only the reflection of the constant-$\theta_i$ angle surface. The existence of flat land is seen as a distinctive characteristic of the IMPES.

A tutorial demonstration of the flat land is shown in Fig. 5. We focus on the transient behavior of Machine 2 in Case-2 as an representation. Note that the following analysis is based on a very simplified demonstration of the IMPES to ensure the simplicity and clearance of expression. The precise modeling of the IMPES is given in the next section.

*Analyzing flat land in the $t$-$\theta$ space*: From Fig. 1 (b), the actual IMTR$_2$ is close to ruler IMTR$_2$ in $t$-$\theta$ space. Under this circumstance, IMPE$_2$ along the system trajectory varies very slightly along the time horizon, as shown in Fig. 2 (b). Machine 2 is a non-critical machine.

*Analyzing flat land in the angle space*: From Fig. 5, since the actual IMTR$_2$ is close to ruler IMTR$_2$ in the $t$-$\theta$ space, the actual system trajectory along the $\theta_2$ axis is also close to the constant-$\theta_2$ angle surface. The IMPE$_2$ along the system trajectory in the angle space varies slightly. For all the system trajectories that are close to the constant-$\theta_2$ angle surface, the IMPE$_2$ along these system trajectories will form a flat land in IMPES$_2$. The energy ball of Machine 2 just rolls in the flat land of IMPES$_2$. Machine 2 is a non-critical machine.

#### 2) MOUNTAINS AND VALLEYS

Following the analysis in Section II C, in the angle space, for a certain system trajectory that goes far from the constant-$\theta_i$ angle surface along the $\theta_i$ axis, the IMPE$_i$ may reach a maximum along the postfault system trajectory. It is likely that the energy ball is climbing over a "mountain". After that step, the machine falls into a "valley", i.e., the instability abyss that lies at the back of the mountain.

The second characteristic of the IMPES is given as follows.

*Mountains and valleys are located on either side of the flat land in each IMPES.*

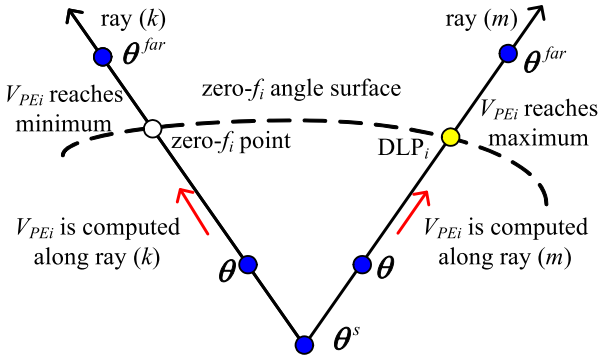


**FIGURE 6.** Modeling of the IMPES using rays.

A demonstration of the mountains and valleys is also shown in Fig. 5. We focus on the transient behavior of Machine 2 in Case-1 for representation.

*Analyzing mountain in the $t$-$\theta$ space*: From Fig. 1 (a), the actual IMTR$_2$ separates from the ruler IMTR$_2$ in $t$-$\theta$ space. Under this circumstance, IMPE$_2$ along the system trajectory may reach a maximum and then become negative infinite along the time horizon, as shown in Fig. 2 (a). Machine 2 becomes unstable.

*Analyzing mountain in the angle space*: From Fig. 5, since the actual IMTR$_2$ separates from the ruler IMTR$_2$ in $t$-$\theta$ space, the system trajectory along the $\theta_2$ axis also goes far from the constant-$\theta_2$ angle surface. The IMPE$_2$ along the system trajectory in the angle space varies severely. For all the system trajectories that leave far from the constant-$\theta_2$ angle surface, the IMPE$_2$ along these system trajectories will form a mountain. The valley is located at the back of the mountain. Mountains and valleys are located on either side of the flat land. The energy ball of Machine 2 goes over the mountain of IMPES$_2$, and it subsequently falls into the valley at the back, i.e., the instability abyss. Machine 2 becomes unstable.

From the analysis above, essentially speaking, the shape of IMPES of Machine that is defined in the angle space, is significantly affected by the constant-$\theta_i$ angle surface. If the system trajectory along $\theta_i$ axis is close to the constant-$\theta_i$ angle surface, it rolls in the flat land with very slight variance of IMPE$_i$; Comparatively, if the system trajectory along $\theta_i$ axis goes far from the constant-$\theta_i$ angle surface, it goes over the mountain and later falls into the valley, i.e., the instability abyss of the machine.

### C. PRECISE MODELING OF IMPES USING RAYS

The modeling of the IMPES in Section B is quite simplified. In order to model the IMPES precisely, the entire angle space should be scanned. In this paper, a fictional linear system trajectory, i.e., ray, is used to compute the IMPE of a machine along it. Assuming that $\boldsymbol{\theta}^{far}$ is a preset point that lies far from $\boldsymbol{\theta}^s$, the ray is depicted as

$$\boldsymbol{\theta} = \alpha(\boldsymbol{\theta}^{far} - \boldsymbol{\theta}^s) + \boldsymbol{\theta}^s \tag{5}$$

In Eq. (5), the ray is formed from $\boldsymbol{\theta}^s$ to $\boldsymbol{\theta}^{far}$ with the variance of $\alpha$. $\alpha$ is the only variable in the equation.

The ray in an individual-machine manner is also redescribed as

$$\theta_i = \alpha(\theta_i^{far} - \theta_i^s) + \theta_i^s \tag{6}$$

A demonstration of the ray is shown in Fig. 6.

From Fig. 6, with the ray rotating in the angle space, the entire angle space is scanned, and the IMPE of a machine along all these rays may form an IMPES. During this rotation, if the ray along the $\theta_i$ axis is close to the constant-$\theta_i$ angle surface, the IMPE$_i$ would be low (flat land occurs); comparatively, if the ray along the $\theta_i$ axis is far from the constant-$\theta_i$ angle surface, the IMPE$_i$ would be high and reach a maximum (mountain occurs). Note that the constant-$\theta_i$ angle surface is a distinctive ray in which $\theta_i^{far}$ is equal to $\theta_i^s$ in the system trajectory.

A tutorial example of the precise modeling of IMPES$_2$ using rays is shown in Fig. 7. ST-A, ST-B and ST-C represent the three different system trajectories in the angle space. We only focus on the behavior of the energy ball of Machine 2 in the IMPES$_2$ as a representation. This case visualizes the analysis in Section B.

From Fig. 7, the shape of the IMPES is established effectively using rays. Flat land, mountains and valleys are clearly found in IMPES$_2$. The IMPES is separated by the flat land because mountains and valleys are located on either side of it.

The motions of the energy ball in the IMPES$_2$ with different tracks are analyzed below.

*Case ST-A (Machine 2 is a non-critical machine)*: The system trajectory along the $\theta_2$ axis is close to the constant-$\theta_2$ angle surface. The energy ball rolls in the flat land with time. Under this circumstance, IMPE$_2$ varies only slightly along ST-A.

*Case ST-B (Machine 2 is an unstable critical machine)*: The system trajectory along the $\theta_2$ axis goes far from the constant-$\theta_2$ angle surface. The energy ball climbs over the mountain and falls into the instability abyss. After that, the IMPE$_2$ becomes negative infinite along ST-B.

*Case ST-C (Machine 2 is a stable critical machine)*: The system trajectory along the $\theta_2$ axis first leaves away from the constant-$\theta_2$ angle surface after a fault occurs, but it inflects back later. Under this circumstance, the energy ball is stopped by the mountain. IMPE$_2$ becomes bounded, although it fluctuates severely along ST-C.

The shape of the IMPES can also be explained in tutorial through the following geological phenomena, as in Figure. 8. In this figure, the ''river'' can be seen as the constant-$\theta_i$ angle surface. The land is close to the river and it is quite flat. The mountains are far from the river and they locate on the either side of the flat land. If the traveler moves close to the river, he is walking on the flat land; comparatively, if he moves far from the river, he has to climb over the mountain. During this free hiking, the real focus of the traveler should be the mountain ridge, i.e., the geological ''boundary'' that characterizes the ''stability'' of the traveler.

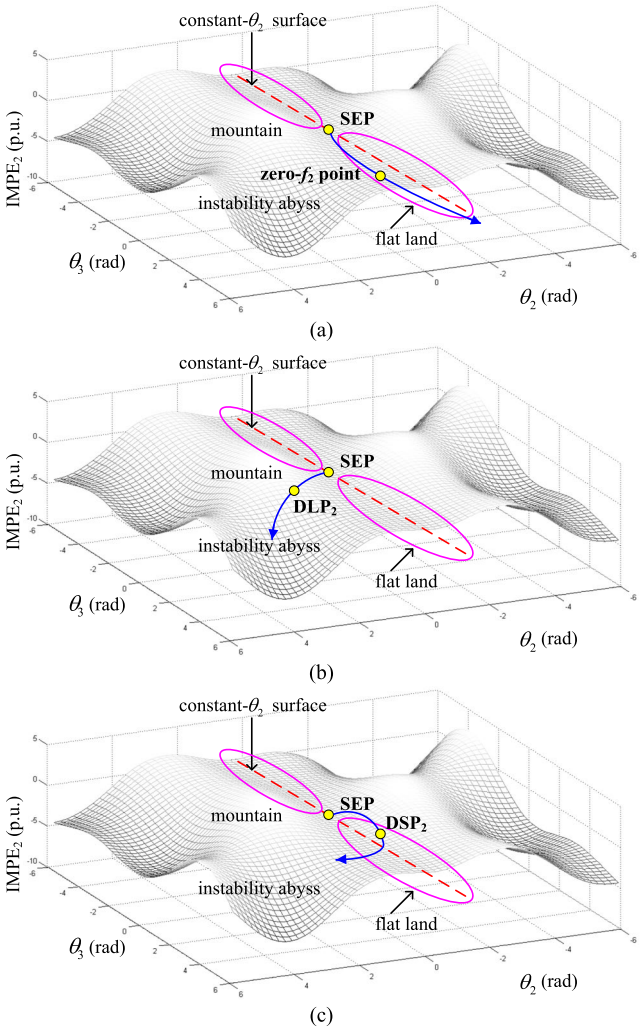


**FIGURE 7.** Motion of an individual-machine energy ball in the IMPES$_3$. (a) Machine 2 is a non-critical machine (ST-A). (b) Machine 2 is an unstable critical machine (ST-B). (c) Machine 2 is a stable critical machine (ST-C).

The analysis above visually demonstrates the transient characteristics of only one individual machine in the multimachine system through the modeling of the IMPES. In the following sections, the transient behaviors of all machines in the multimachine system will be depicted using multiple IMPESs.

### D. TRANSIENT BEHAVIOR OF A MULTI-MACHINE SYSTEM USING MULTIPLE IMPESs

Following the analysis above, for a multimachine system, each individual machine corresponds to its unique IMPES. It should be noted that each IMPES is modeled independently. IMPES$_i$ only describes the transient characteristics of Machine $i$ itself. It is meaningless to observe the transient characteristics of another machine in IMPES$_i$.

Under a certain system trajectory after a fault occurs, each energy ball rolls in its corresponding IMPES in parallel. Following the definition of the IMPES, the track of each ball is for the same system trajectory. However, since the shape of each IMPES is unique and different, the transient characteristics of each energy ball are also different.

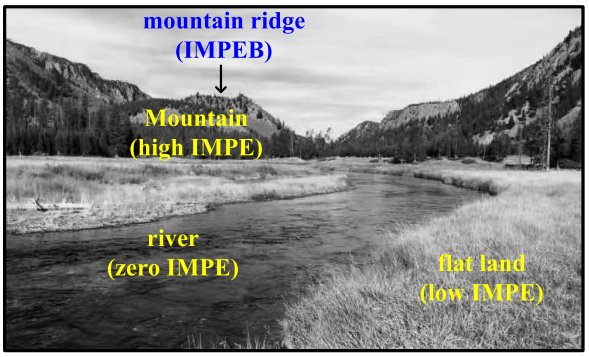


**FIGURE 8.** Explanation of the shape of IMPES in tutorial.

A tutorial demonstration of the transient characteristics of each energy ball in its IMPES in a multimachine system is shown in Fig. 9. The analysis below is still based on the simplified modeling of IMPES for clearance.

From Fig. 9, the energy ball of each machine rolls in parallel in its corresponding IMPES after a fault occurs. Although the tracks of the two energy balls are the same system trajectory, the shapes of the two IMPESs are completely different. In particular, because the constant-$\theta_2$ angle surface and constant-$\theta_3$ angle surface are perpendicular in the $\theta_2$-$\theta_3$ angle space, as in Fig. 9, the shapes of the two IMPESs also seem ''perpendicular''.

The transient behavior of Machines 2 and 3 are described as follows:

*Behavior of Machine 2*: The system trajectory along the $\theta_2$ axis is close to the constant-$\theta_2$ angle surface. The energy ball of Machine 2 rolls in the flat land of IMPES$_2$; thus, Machine 2 is a non-critical machine.

*Behavior of Machine 3*: The same system trajectory along the $\theta_3$ axis goes far from the constant-$\theta_3$ angle surface (although it is close to the constant-$\theta_2$ angle surface along the $\theta_2$ axis). The energy ball of Machine 3 goes over the mountain in IMPES$_3$; thus, Machine 3 becomes an unstable critical machine.

The analysis above is based on the simplified expression of the IMPES. It can be further demonstrated by using the precise modeling. Case-2 with the precise modeling of each IMPES is given below. The corresponding transient stability analysis in the $t$-$\theta$ space is already given in Fig. 1 (b). Using TS-4 as the test bed, the IMPESs of the three machines are shown in Figs. 10 (a) to (c). Note that the IMPES of Machine 1 is also given in the figure, although $\theta_1$ is not independent in the COI-SYS reference.

From Fig. 10, each energy ball rolls in parallel in its corresponding IMPES, and the track of each ball is for the same system trajectory. The flat land, mountains and valleys are found in each IMPES. However, the shape of each IMPES is different. Therefore, the transient performance of each energy balls is completely different. In particular, for Case-2, the energy ball of Machine 3 already goes over the mountain

at $DLP_3$ and becomes unstable at 0.369 s in $IMPES_3$. Comparatively, at the same moment, the energy ball of Machine 2 is still rolling in the flat land in $IMPES_2$, although the two energy balls of Machines 2 and 3 have the same system trajectory.

At first glance, it seems that the IMPES of each machine is modeled in an ''isolated'' manner. In fact, this is a misunderstanding because all machines interact with each other in the transient stability of the multi-machine system. In particular, The IMPES of Machine $i$ is modeled based on $f_i(\theta)$ that comprises of $\theta$ of all machine in the system, as analyzed in Section II A. Therefore, The IMPES is modeled and depicted ''independently'' rather than ''isolated''.

The analysis above shows that constant-$\theta_i$ angle surface has significant effect to the shape of each IMPES. In fact, compared with observing the individual-machine energy ball rolling within the flat land (the non-critical machine case), the real focus of the system operator should be the transient behavior of the energy ball climbing over the mountain ''ridge'', i.e., the ''stability boundary'' of the machine. This is addressed in the following sections.

## IV. INDIVIDUAL-MACHINE POTENTIAL ENERGY BOUNDARY

### A. ZERO-F ANGLE SURFACE

Following the analysis in Section III, from the perspective of IMPES, the machine becoming unstable is described as the energy ball of the machine leaving far from the flat land and then climbing over the mountain. Clearly, a stability boundary can be found in the angle space to describe the key change of the individual-machine energy ball from maintaining stable to becoming unstable when the ball goes over the mountain. This also leads to the emergence of the second question: what is the individual-machine potential energy boundary (IMPEB)?

A tutorial example is given below to demonstrate the mechanism of the IMPEB. In this case, we still first focus on the transient characteristics of Machine 2 in $IMPES_2$ for representation. The variance of the $IMPE_2$ in the $t$-$V$ space in Case-1 and Case-2 is already given in Fig. 2. The system trajectories of the two cases in the angle space are shown in Fig. 11. The Kimbark curves of Machine 2 in the two cases are also shown in Fig. 12.

#### 1) MOUNTAIN RIDGE (CASE-1)

*Analyzing mountain ridge in the t-V space and θ-f space*: From Fig. 2 (a), for Case-1, $IMPE_2$ first reaches a maximum at $DLP_2$. After that step, $IMPE_2$ decreases, and the machine becomes unstable. In this case, Machine 2 is a typical unstable critical machine because the Kimbark curve of Machine 2 shows a very clear ''accelerating-decelerating'' characteristic, as in Fig. 12 (a).

*Analyzing mountain ridge in the angle space*: If we observe the transient behavior of Machine 2 from the IMPES perspective, $DLP_2$ is located on the ''ridge'' of the mountain.

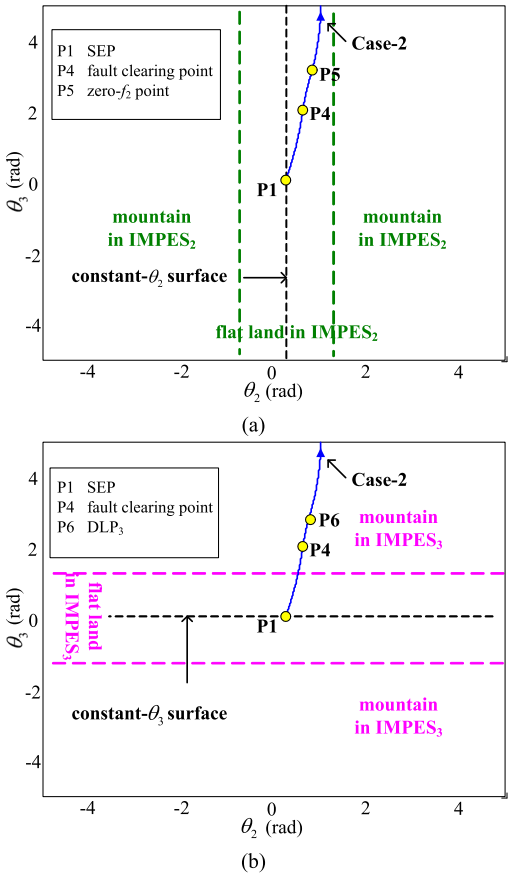


**FIGURE 9.** Transient characteristics of each machine using simplified IMPES. (a) $IMPES_2$. (b) $IMPES_3$.

This ''ridge'' is definitely seen as the individual-machine potential energy boundary of Machine 2 ($IMPEB_2$). Once the system trajectory goes through $IMPEB_2$, $DLP_2$ is the intersection point, as shown in Fig. 11. After that, Machine 2 falls into the instability abyss, and it becomes unstable.

Following the definition of DLP, $IMPEB_2$ is mathematically denoted as

$$f_2(\boldsymbol{\theta}) = 0 \tag{7}$$

In this paper, we name the angle surface that satisfies Eq. (7) as the ''zero-$f_i$'' angle surface. Each machine corresponds to its unique zero-$f_i$ angle surface.

A tutorial demonstration of the zero-$f_2$ angle surface is shown in Fig. 11. Compared with the constant-$\theta_i$ angle surface that affects the shape of the IMPES, the zero-$f_i$ angle surface is of key value because it essentially depicts the stability boundary of the machine.

#### 2) PIT BOTTOM (CASE-2)

Following Eq. (7), at first glance, it seems like the zero-$f_i$ angle surface can be directly defined as the IMPEB. However, the situation may become quite complicated under certain circumstances. In particular, the IMPE of the machine might reach ''minimum'', i.e., the ''pit bottom'' rather than the

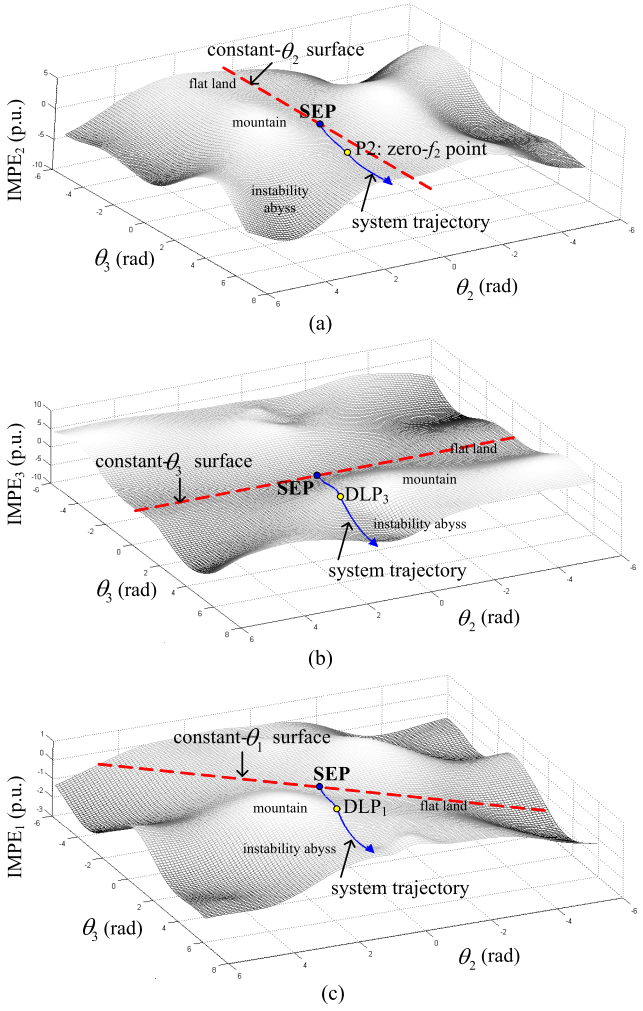


**FIGURE 10.** Shape of each IMPES in a multimachine system. (a) IMPES$_2$. (b) IMPES$_3$. (c) IMPES$_1$.

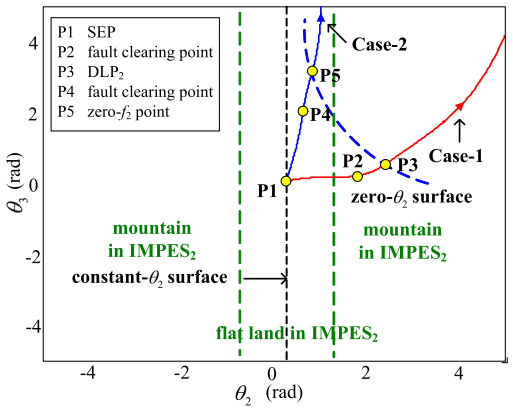


**FIGURE 11.** Demonstration of the zero-$f_2$ angle surface.

"maximum" when $f_i$ of the machine is equal to zero. The analysis is given below.

*Analyzing pit bottom in the t-V space and θ-f space*: From Fig. 2 (b), for Case-2, IMPE$_2$ varies slightly along the time horizon, and it reaches a "minimum" at P5 at 0.42 s. However, it is worth pointing out that $f_2$ is also equal to zero at

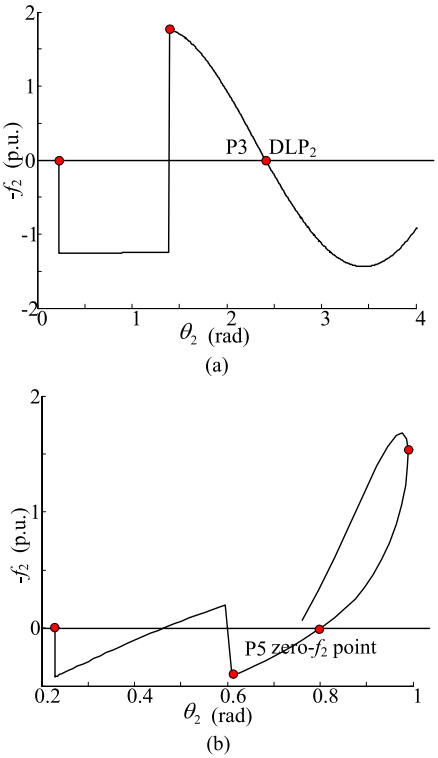


**FIGURE 12.** Kimbark curve of Machine 2. (a) Case-1. (b) Case-2.

this point. In this case, Machine 2 is a non-critical machine because the Kimbark curve of Machine 2 does not show a clear "accelerating-decelerating" characteristic, as shown in Fig. 12 (b).

*Analyzing pit bottom in the angle space*: Compared with Case-1 that Machine 2 goes over the mountain ridge in IMPES$_2$, in this case, the energy ball of Machine 2 is rolling in the flat land. However, the system trajectory still goes through the zero-$f_2$ surface, and the intersection point is P5, as in Figs. 11. Under this circumstance, IMPE$_2$ reaches "minimum" at P5 rather than maximum, and the energy ball of Machine 2 falls in the "pit bottom" in the IMPES$_2$.

In this paper, we name P5 in Fig. 11 the "zero-$f_i$ point". The zero-$f_i$ point can be found in the Kimbark curve of a stable critical machine or a non-critical machine. The zero-$f_i$ point represents the "pit bottom point" where the "minimum" IMPE occurs.

From the analysis above, one naturally obtains the following:

*The IMPEB$_i$ is part of the zero-$f_i$ angle surface.*

This deduction naturally leads to an idea that the IMPEB of Machine $i$ should be "cut" from its corresponding zero-$f_i$ angle surface. Detailed analysis will be given in Section C.

### B. STABILITY CHARACTERIZATION USING THE ZERO-F ANGLE SURFACE

Along each ray in the angle space, the extrema (minimum or maximum) of the IMPE of Machine $i$ satisfies

$$\frac{dV_{PEi}}{d\alpha} = \frac{dV_{PEi}}{d\theta_i}\frac{d\theta_i}{d\alpha} = 0 \tag{8}$$

Eq. (8) is further expressed as

$$f_i(\boldsymbol{\theta})(\theta_i - \theta_i^s) = 0 \tag{9}$$

Eq. (9) can be simplified as

$$f_i(\boldsymbol{\theta}) = 0 \tag{10}$$

Eq. (10) is the mathematical expression of the zero-$f_i$ angle surface using rays. The IMPE of Machine $i$ reaches extrema (minima or maxima) when the system trajectory goes through the zero-$f_i$ angle surface. From Eq. (10), the mathematical expression of the zero-$f_i$ angle surface using rays is exactly the same as that along the actual system trajectory as in Eq. (7).

Following the analysis in Section A, the characteristics of the zero-$f_i$ angle surface are summarized as follows:

(i) The zero-$f_i$ angle surface only requires $f_i$ to be zero.

(ii) The IMPE$_i$ might reach a ''maximum'' or ''minimum'' at the zero-$f_i$ angle surface.

(iii) Following (ii), from the IMPES perspective, a zero-$f_i$ angle surface might occur on a ''mountain ridge'' or in a ''pit bottom'' in the IMPES.

(iv) The DLP$_i$ or zero-$f_i$ point is the intersection point between the actual postfault system trajectory and the zero-$f_i$ angle surface.

(v) The zero-$f_i$ surface would occur repeatedly in the angle space (detailed analysis is given in Section VI).

Case-2 is used to demonstrate the multiple zero-$f_i$ surfaces with the precise modeling of the IMPES in a multi-machine system. The zero-$f_i$ angle surface of each machine is shown in Figs. 13 (a) to (c). The IMPES in each figure is demonstrated in contour form (detailed 3D modeling is already given in Fig. 10). The purple line in the figure is the constant-$\theta_i$ surface of each machine. The green line is the actual system trajectory in $\theta_2$-$\theta_3$ angle space.

In Fig. 13, the energy ball of each machine moves in parallel in its corresponding IMPES. The tracks of the three balls are the same system trajectory. By using the zero-$f_i$ angle surface, the performance of each machine in its corresponding IMPES is analyzed as follows:

*Case of Machine 2*: After fault clearing, the energy ball of Machine 2 rolls in the flat land of IMPES$_2$. Under this circumstance, IMPE$_2$ varies slightly along system trajectory. IMPE$_2$ reaches a minimum at the zero-$f_2$ point (P5 as in Fig. 11), which is the intersection point between the zero-$f_2$ surface and the system trajectory. Machine 2 is definitely a non-critical machine

*Case of Machine 3*: the energy ball of Machine 3 goes over a mountain in IMPES$_3$. IMPE$_3$ reaches a maximum at DLP$_3$, which is the intersection point between the zero-$f_3$ surface and the system trajectory. After that step, Machine 3 falls into the valley, i.e., the instability abyss in IMPES$_3$, and it becomes unstable.

*Case of Machine 1*: the energy ball of Machine 1 goes over a mountain in IMPES$_1$. IMPE$_1$ reaches a maximum at DLP$_1$, which is the intersection point between the zero-$f_1$ surface and the system trajectory. After that step, Machine 1 becomes unstable.

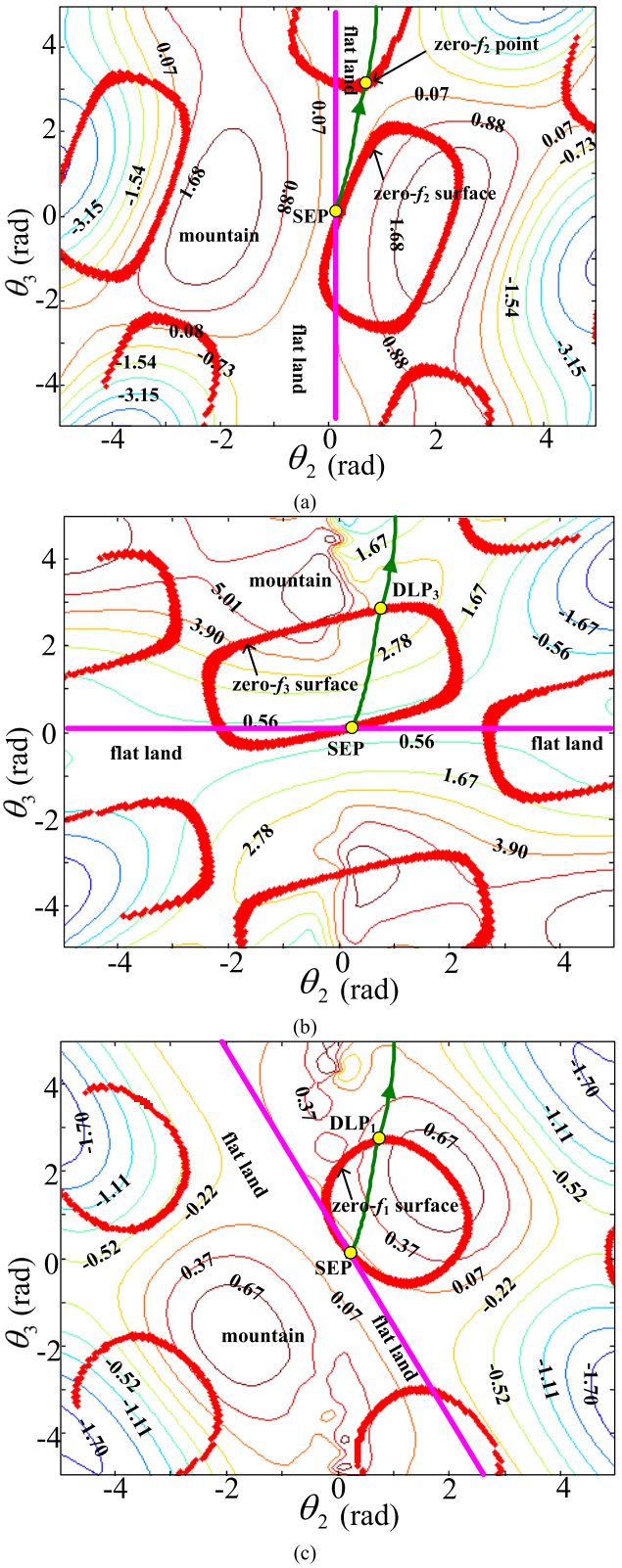


**FIGURE 13.** Zero-$f_i$ surface in a multimachine system. (a) Zero-$f_2$ surface. (b) Zero-$f_3$ surface. (c) Zero-$f_1$ surface.

From the analysis above, once the fault is cleared, the system trajectory goes through the zero-$f_i$ surface of each individual machine one after another along the time horizon. In particular, the system trajectory goes through the zero-$f_1$ surface, zero-$f_3$ surface and zero-$f_2$ surface at 0.36 s, 0.38 s and 0.42 s, as shown in Fig. 13. The IMPE of each machine in the system would reach extrema (maxima or minima) at the intersection point between the system trajectory and each zero-$f_i$ surface.

The complication of the zero-$f_i$ angle surface fully indicates that it *cannot* be used directly as the IMPEB. Therefore, a procedure should be found to cut the IMPEB from the zero-$f_i$ angle surface.

### C. SCISSOR ANGLE SURFACE

From the analysis in Section B, using rays, the IMPEB that depicts the maximum IMPE is denoted as

$$\begin{cases} \dfrac{dV_{PEi}}{d\alpha} = 0 \\ \dfrac{d^2V_{PEi}}{d^2\alpha} < 0 \end{cases} \Rightarrow \begin{cases} f_i(\boldsymbol{\theta}) = 0 \\ \dfrac{d^2V_{PEi}}{d^2\alpha} < 0 \end{cases} \tag{11}$$

From Eqs. (10) and (11), the IMPEB is also an angle-surface function, and it is part of the zero-$f_i$ angle surface.

Since IMPEB$_i$ is part of the zero-$f_i$ angle surface, it can be cut by using a "scissor". This angle surface is denoted as

$$\frac{d^2V_{PEi}}{d^2\alpha} = \left(\theta_i^{far} - \theta_i^s\right) \frac{df_i(\boldsymbol{\theta})}{d\boldsymbol{\theta}} \frac{d\boldsymbol{\theta}}{d\alpha} = 0 \tag{12}$$

Eq. (12) is further described as

$$\left(\theta_i - \theta_i^s\right) \sum\nolimits_{h=1}^{n} \frac{\partial f_i}{\partial \theta_h} \left(\theta_h - \theta_h^s\right) = 0 \tag{13}$$

In this paper, we define the angle surface that satisfies Eq. (13) as the "scissor angle surface" of Machine $i$. From the equation, the scissor angle surface is further described as a combination of the two angle surfaces. In particular, the first surface is only the constant-$\theta_i$ angle surface ($\theta_i = \theta_i^s$) as in Eq. (4), while the second-scissor-angle-surface (SSAS) can be denoted as

$$\sum\nolimits_{h=1}^{n} \frac{\partial f_i}{\partial \theta_h} \left(\theta_h - \theta_h^s\right) = 0 \tag{14}$$

From Eq. (14), the SEP lies in the SSAS of each machine.

A demonstration of the SSAS of each machine is shown in Fig. 14. In the figure, the purple line is the constant-$\theta_i$ angle surface. The green line is the SSAS of the machine. The red line is the IMPEB. The blue line is the remaining part of the zero-$f_i$ surface.

From Fig. 14, compared with the straight line of the constant-$\theta_i$ angle surface, the shape of the SSAS of the machine is rather irregular and it spreads over the entire angle space of the multimachine system. By using the scissor angle surface, it is clear that the zero-$f_i$ surface of each individual machine is cut into two parts, and thus the IMPEB of each machine is eventually obtained. If the system trajectory goes through the IMPEB$_i$, the intersection point would be DLP$_i$, and Machine $i$ would become unstable.

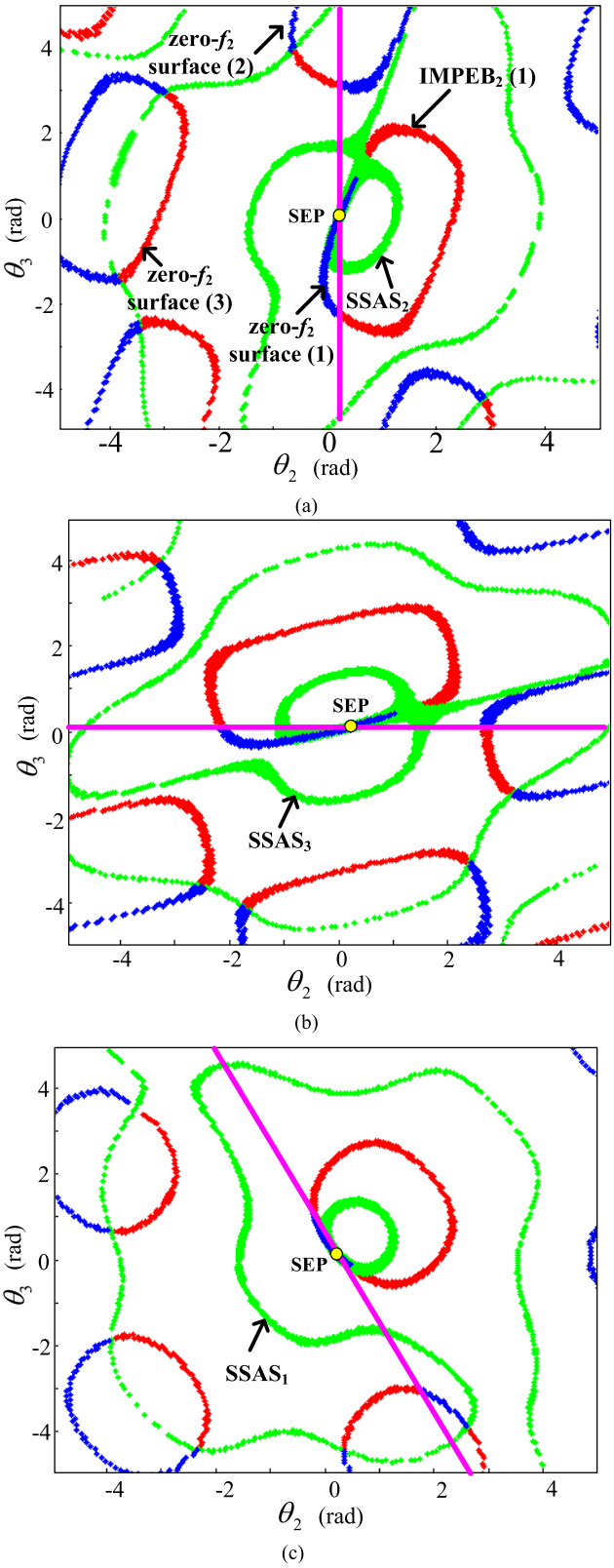


**FIGURE 14.** SSAS of an individual machine. (a) SSAS$_2$. (b) SSAS$_3$. (c) SSAS$_1$.

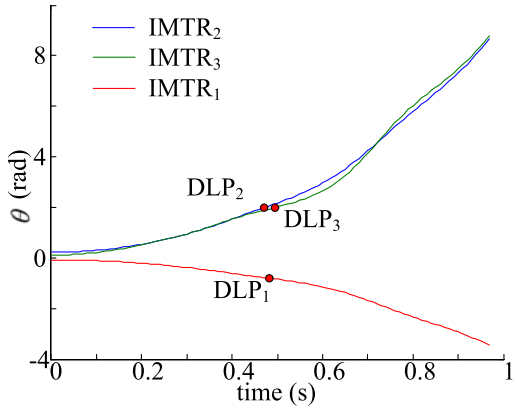


**FIGURE 15.** System trajectory [TS-4, bus-1, 0.40 s].

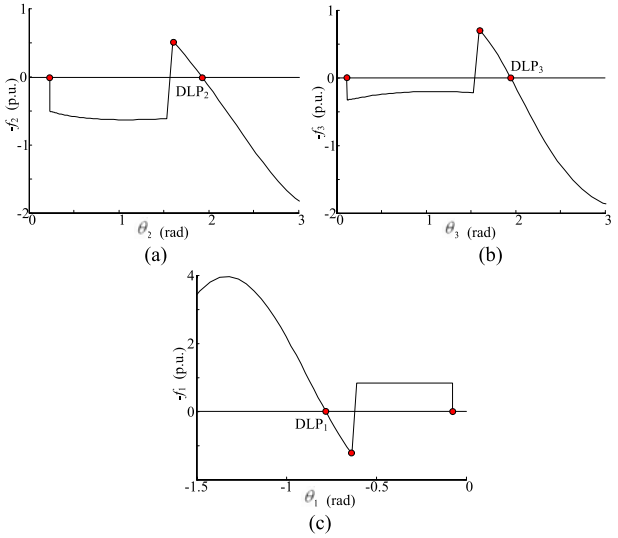


**FIGURE 16.** Simulated Kimbark curves [TS-4, bus-1, 0.40 s]. (a) Kimbark curve of Machine 2. (b) Kimbark curve of Machine 3. (c) Kimbark curve of Machine 1.

In the following analysis, the proposed IMPES and IMPEB in this paper will be systematically demonstrated through the concepts and phenomena in the individual-machine studies. This demonstration may help readers gain deep insights into individual-machine transient energy conversion in a multimachine system through the perspective of the IMPES.

## V. CASE STUDY

### A. REEXPLANATION OF LEADING UNSTABLE MACHINE

#### 1) TEST BED

In the IMEAC method, the leading unstable machine (LUM) is defined as the unstable critical machine whose DLP occurs first among all unstable critical machines in the system. The concept of LUM is of key importance in the IMEAC method because it is identical to the leading loss-of-synchronism point (LOSP) of the system [8], [9]. In the following analysis, the LUM is re-explained using IMPEB.

Case-3 [TS-4, bus-1, 0.40 s] is given below. In this case all machines are unstable critical machines. The system trajectory is shown in Fig. 15. The Kimbark curves of the machines are shown in Figs. 16 (a) to (c). The IMPEB of each critical machine is shown in Fig. 17. Note that all the IMPEBs of the individual machines in the system are plotted in one figure for simplicity and clearance. Physically, the three IMPEBs should be analyzed in parallel. The colors in Fig. 17 are the same as those in Fig. 14. The variance of the IMPE along time horizon is shown in Fig. 18.

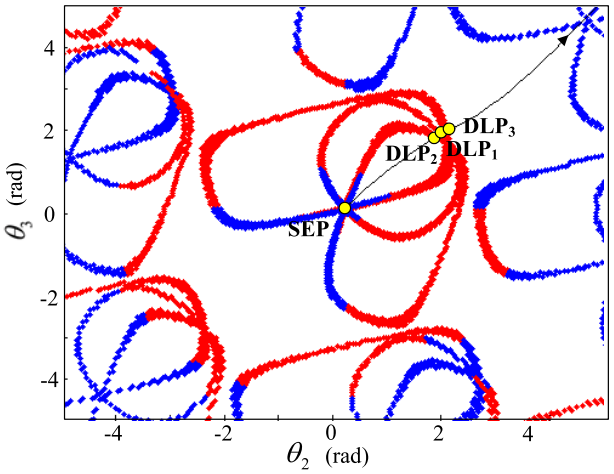


**FIGURE 17.** IMPEBs of the three machines in the system.

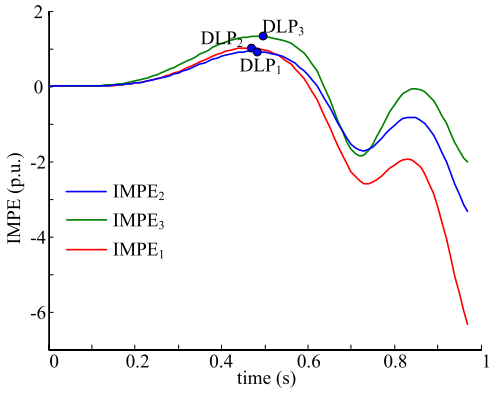


**FIGURE 18.** Variance of IMPE of each machine along the time horizon.

#### 2) IMEAC ANGLE

From Figs. 15 and 16, using IMEAC [8], $DLP_2$, $DLP_1$, and $DLP_3$ occur at 0.47 s, 0.48 s and 0.49 s, respectively. Therefore, Machine 2 is defined as the LUM in this case because it first becomes unstable and further causes the system to become unstable following the unity principle.

#### 3) IMPES ANGLE

From the perspective of IMPES, each individual-machine energy ball rolls in its corresponding IMPES in parallel. Detailed analysis is shown as below.

*Behavior of Machine 2*: The energy ball of Machine 2 climbs the mountain after a fault occurs. The system trajectory goes through $IMPEB_2$ at 0.47 s. The intersection point is $DLP_2$, and $IMPE_2$ reaches a maximum at $DLP_2$. $DLP_2$ occurs at 0.47 s. Machine 2 goes unstable.

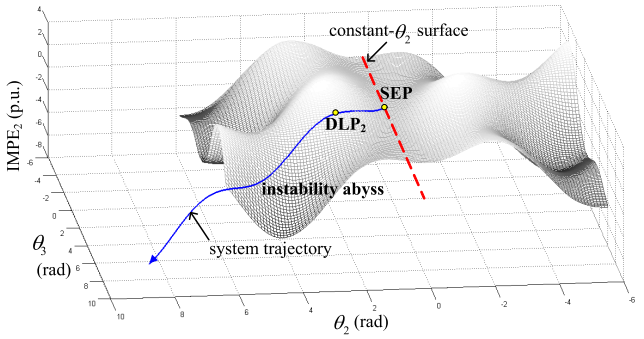


**FIGURE 19.** Instability abyss in $IMPES_2$.

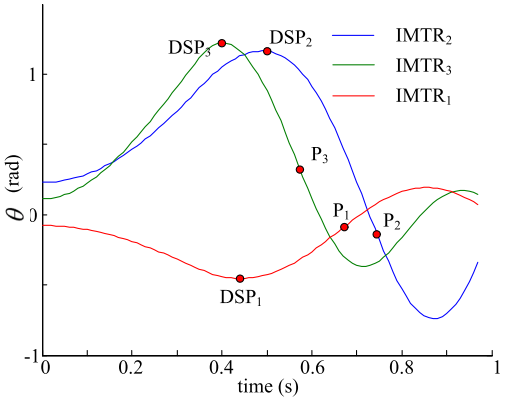


**FIGURE 20.** System trajectory [TS-4, bus-6, 0.35 s].

*Behavior of Machine 1*: The system trajectory goes through $IMPEB_1$ at 0.48 s. The intersection point is $DLP_1$, and $IMPE_1$ reaches a maximum at $DLP_1$. $DLP_1$ occurs at 0.48 s. Machine 1 goes unstable.

*Behavior of Machine 3*: The system trajectory goes through $IMPEB_3$ at 0.49 s. The intersection point is $DLP_3$, and $IMPE_3$ reaches a maximum at $DLP_3$. $DLP_3$ occurs at 0.49 s. Machine 3 goes unstable.

From the analysis above, since the system trajectory goes through $IMPEB_2$ first, Machine 2 is defined as the LUM, and the instability of Machine 2 first causes the instability of the system according to the unity principle. After that step, the energy ball of Machine 2 would fall into a deep valley, i.e., the instability abyss in the $IMPES_2$ as in Fig. 19. This outcome also incurs $IMPE_2$ to become negative infinite with time, as in Fig. 18. Therefore, from the perspective of IMPES, a machine can be defined as the LUM if the system trajectory goes through its corresponding IMPEB first along time horizon.

### B. ANALYZING STABLE SYSTEM TRAJECTORY USING IMPES

#### 1) TEST BED

Case-4 [TS-4, bus-6, 0.35 s] is used to demonstrate the transient characteristic of the stable system trajectory in the IMPES if the system trajectory does not go through any IMPEB. The system trajectory is shown in Fig. 20. The Kimbark curves of the machines are shown in Figs. 21 (a) to (c).

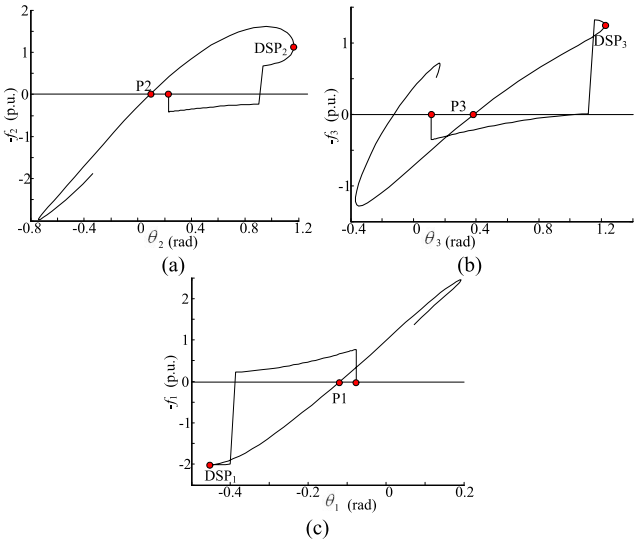


**FIGURE 21.** Simulated Kimbark curves [TS-4, bus-6, 0.35 s]. (a) Kimbark curve of Machine 2. (b) Kimbark curve of Machine 3. (c) Kimbark curve of Machine 1.

The IMPEB of each critical machine is shown in Fig. 22. The denotation of colors of the lines in the figure is the same as that in Fig. 14. The variance of the IMPE is shown in Fig. 23.

#### 2) IMEAC ANGLE

From Figs. 20 and 21, taking Machine 2 as an example, the Kimbark curve of the machine inflects back at $DSP_2$, where $\theta_2$ reaches a maximum. After that step, the machine accelerates in an opposite direction in the second swing. The Kimbark curve goes through the zero-$f_2$ point (P2). Later, the machine decelerates again, as shown in Fig. 21 (a). The other two machines also show similar transient behaviors.

#### 3) IMPES ANGLE

From the perspective of IMPES, each energy ball rolls in parallel in its corresponding IMPES. The system trajectory climbs towards the mountain in the IMPES of each machine after fault clearing. Unfortunately, the individual-machine kinetic energy (IMKE) of each critical machine is exhausted at its DSP. Therefore, the system trajectory goes through $DSP_3$, $DSP_1$, and $DSP_2$, and the entire system trajectory inflects back at $DSP_2$ at 0.50 s because $DSP_2$ occurs the latest among all DSPs in the system. After that step, the system trajectory goes through P3 first. At this point, $IMPE_3$ reaches a local minimum and thus P3 is the zero-$f_3$ point. Later, $IMPE_1$ and $IMPE_2$ also reach a minimum when the system trajectory reaches P1 and P2 in their corresponding IMPESs, respectively, as shown in Fig. 22. P1, P2 and P3 are also the "pit bottom" in the corresponding IMPESs.

Finally, we emphasize again that the IMPES of each individual machine should be modeled independently and the transient behaviors of the individual-machine energy ball in each IMPES should be analyzed in parallel. Plotting all IMPEBs in the system in one figure, as shown in Figs. 17 and 22, is just for simplicity and clearance.

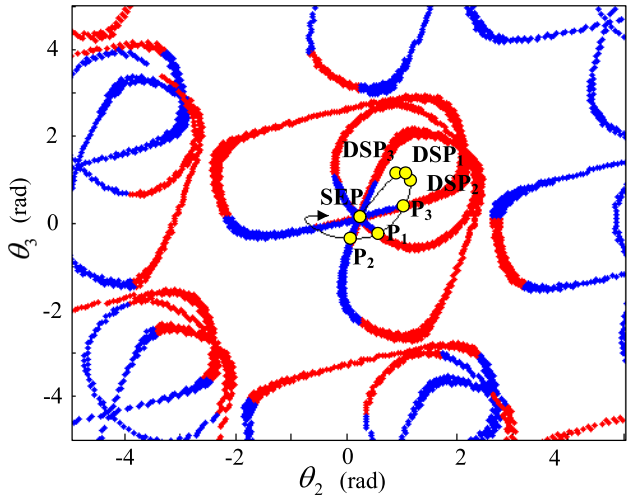


**FIGURE 22.** IMPEBs of the three machines in the system.

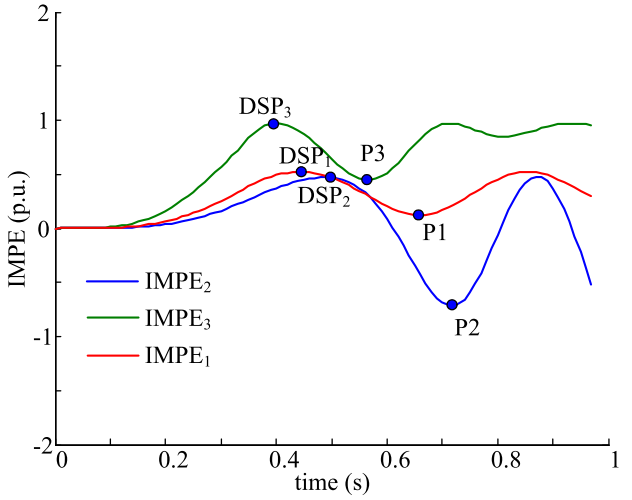


**FIGURE 23.** Variance of IMPE of each machine along time horizon [TS-4, bus-6, 0.35 s].

### C. MULTI-SWING INSTABILITY OF AN INDIVIDUAL MACHINE

#### 1) TEST BED

The concept of IMPEB can also be used to explain the phenomena of the multiswing instability of an individual machine. This case is seen as the retrospect of the potential energy ridge proposed by Ando [7]. The fault is [TS-5, bus-1, 0.40 s]. The system trajectory is shown in Fig. 24. The Kimbark curve of Machine 3 is shown in Fig. 25. The $IMPEB_3$ is shown in Fig. 26. The denotation of colors in the figure are the same as that in Fig. 14. In this case we only focus on the transient behavior of the LUM, i.e., Machine 3 for representation.

#### 2) IMEAC ANGLE

From Figs. 24 and 25, Machines 1 and 3 both become second-swing unstable, while Machine 2 becomes third-swing unstable. Machine 3 is defined as LUM because $DLP_3^{(2)}$ occurs the first among all DLPs along the time horizon at

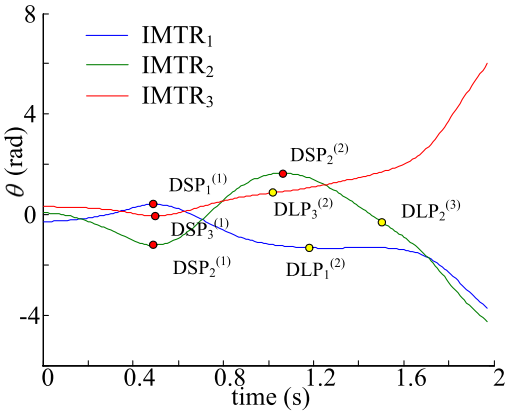


**FIGURE 24.** System trajectory [TS-5, bus-1, 0.40 s].

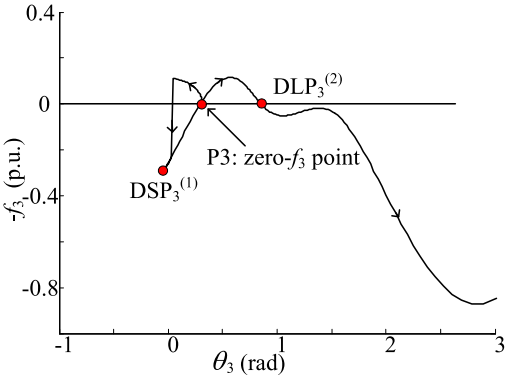


**FIGURE 25.** Kimbark curve of Machine 3 [TS-5, bus-1, 0.40 s].

1.02 s. The system becomes unstable at $DLP_3^{(2)}$ according to the unity principle.

#### 3) IMPES ANGLE

We observe the transient characteristics of Machine 3 by using IMPEB. In the first swing, the system trajectory fails to go through $IMPEB_3^{(1)}$, which lies on the right side of the SEP, and it inflects back at $DSP_3^{(1)}$. After that step, the system trajectory finally goes through $IMPEB_3^{(2)}$, which lies on the left side of the SEP, and the intersection point is $DLP_3^{(2)}$. At this point, the machine finally becomes unstable, causing the system to become unstable following the unity principle. Therefore, compared with the classic potential energy ridge [7], the multiswing transient characteristics of the machine are clearly described by using IMPEB as proposed in this paper.

### D. TRANSIENT ANALYSIS OF THE NEW ENGLAND SYSTEM USING IMPES

The concept of IMPES can also be extended to a larger-scale TS-1 system with ten machines. The system trajectory is shown in Fig. 27 (a). The variance of the IMPE of each critical machine in the $t$-$V$ space is shown in Fig. 28. Machine 5 becomes unstable in this case.

From Figs. 27 and 28, in this simulation case, the IMPES of each machine in the TS-1 system becomes a 10-dimensional hypersurface (the angle space of TS-1 is 9 dimensions). Although the IMPES of each machine cannot be visualized,

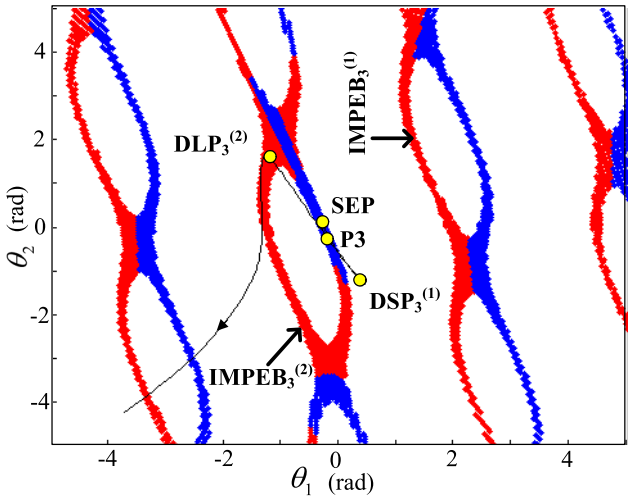


**FIGURE 26.** **IMPEB$_3$ in the TS-5.**

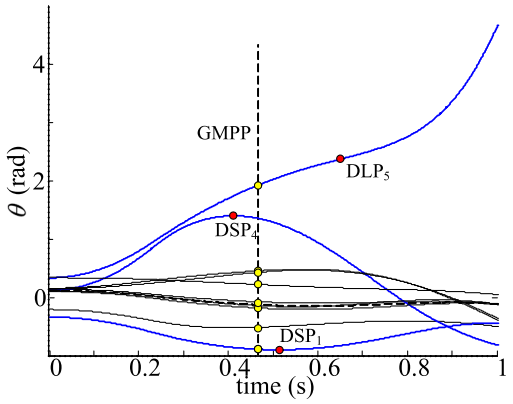


**FIGURE 27.** **System trajectory [TS-1, bus-19, 0.230s].**

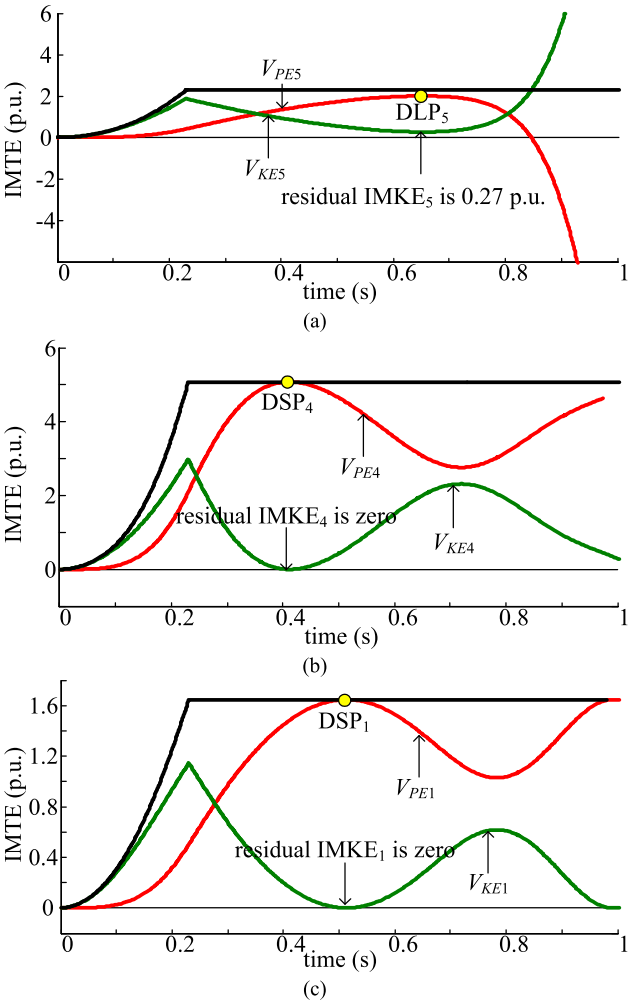


**FIGURE 28.** **Transient energy conversion inside each critical machine [TS-1, bus-19, 0.230 s]. (a) Machine 5. (b) Machine 4. (c) Machine 1.**

it can still be observed partially in the $t$-$V$ space. From Fig. 28, each individual-machine energy ball rolls in its IMPES in parallel and this motion can be clearly observed through the variance of the IMPE along time horizon. In particular, the energy ball of Machine 5 goes over the mountain at DLP$_5$ and falls in the instability abyss in IMPES$_5$. Comparatively, the energy ball of Machine 4 inflects back at DSP$_4$ before reaching the mountain ridge in the IMPES$_4$. Meanwhile, each non-critical machine rolls slightly in the flat land in its corresponding IMPES.

A tutorial demonstration about the transient behavior of Machine 5 in the IMPES$_5$ is shown in Fig. 29. The critically stable and critically unstable cases are also given for comparisons in the figure. Detailed analysis about the critically stable case is already given in Ref. [11]. From the figure, the system should be evaluated to go unstable when system trajectory goes through IMPEB$_5$ (the intersection point is DLP$_5$) rather than global PEB (the intersection point is GMPP in Fig. 27).

The simulation cases above already systematically demonstrate the fundamental concepts of IMPES. In the next section, complicated concepts and distinctive phenomena in the global method and the IMEAC method will be theoretically explained by using IMPES.

## VI. EXPLANATIONS TO THE CLASSIC TRANSIENT CONCEPTS USING IMPES

### A. ETERNAL-ACCELERATION OF A CRITICAL MACHINE

In the IMEAC method [8]–[10], the Kimbark curve of an unstable critical machine generally shows a clear ''accelerating-decelerating'' characteristic after the fault occurs. However, distinctive phenomena might be observed in very rare simulation environments. That is, an unstable machine shows an ''eternal-accelerating'' characteristic without deceleration in the first swing.

The system trajectories and corresponding Kimbark curves of machines with different faults are shown in Figs. 30 and 31, respectively. From Fig. 31, one can find that the Kimbark curve of Machine 3 along ST-1 shows a typical ''accelerating-decelerating'' characteristic. However, the Kimbark curve of Machine 3 along ST-2 is always lower than the zero-$f_3$ line after the fault occurs, which indicates that Machine 3 continues to accelerate along ST-2.

This phenomena can be explained by using the concept of IMPES. The IMPES of Machine 3 and the contour map are shown in Figs. 32 and 33, respectively. The values in the

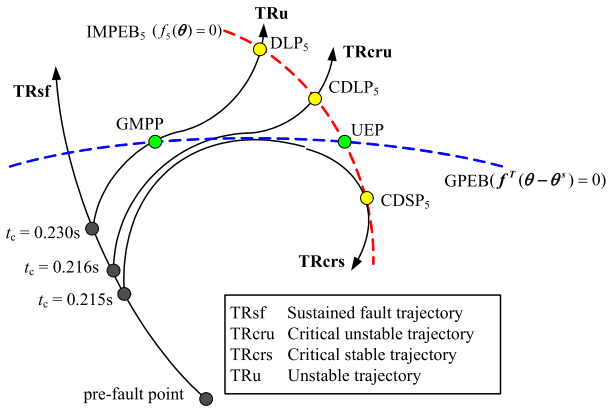


**FIGURE 29.** Demonstration about the unstable system trajectory going through IMPEB$_5$.

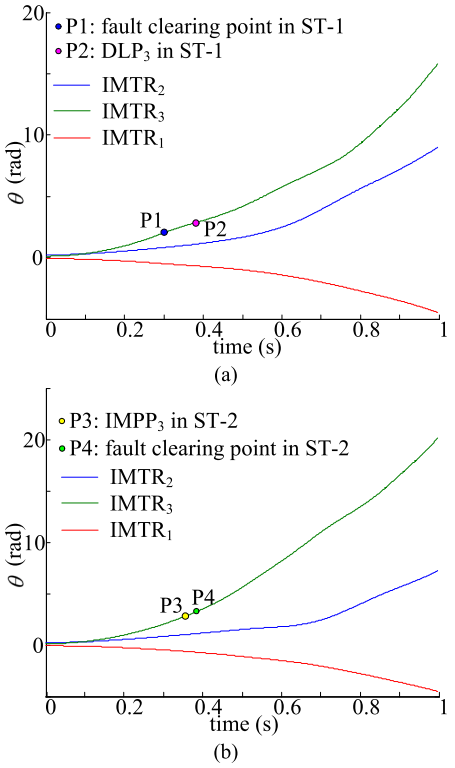


**FIGURE 30.** System trajectories. (a) System trajectory-1 (ST-1) [TS-4, bus-9, 0.300 s]. (b) System trajectory-2 (ST-2) [TS-4, bus-9, 0.380 s].

contour map can be found in Fig. 13. The variance of IMPE$_3$ along time horizon is shown in Fig. 34. In this case we only focus on the transient behavior of Machine 3 in the IMPES$_3$.

Detailed analysis is given as follows.

*Case ST-1*: The fault clearing point (P1) of ST-1 occurs at 0.300 s. After that step, the energy ball of Machine 3 still needs to climb up the mountain in IMPES$_3$, and the system trajectory goes through IMPEB$_3$ at DLP$_3$ (P2) at 0.384 s, as shown in Fig. 32. Under this circumstance, the "deceleration area" can be clearly found in the Kimbark curve of the machine. In particular, the motion of the energy ball from P1 to P2 in IMPES$_3$ directly corresponds to the "deceleration area" of the Kimbark curve of Machine 3.

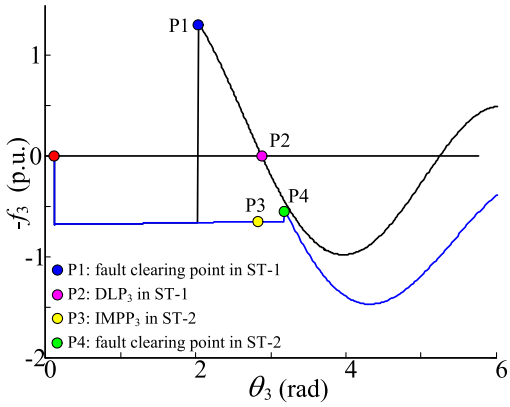


**FIGURE 31.** Kimbark curves of Machine 3 with ST-1 and ST-2.

*Case ST-2*: Compared with the case in ST-1, this case becomes more complicated. After the fault occurs, the energy ball keeps accelerating in IMPES$_3$, and the system trajectory goes through IMPEB$_3$ at 0.362 s. At this moment, IMPE$_3$ reaches a maximum at the individual-machine maximum potential energy point (IMPP) of Machine 3 (P3). In fact, the system trajectory from SEP to IMPP$_3$ is identical to the "sustained-fault" trajectory because the fault is not cleared. Once the system trajectory goes through IMPP$_3$, the energy ball falls into the valley (instability abyss) until it reaches the fault clearing point (P4), as shown in Fig. 33. Unfortunately, at this moment, the energy ball already lies at the back of the mountain, i.e., the instability abyss, as shown in Figs. 32 and 33. Therefore, the energy ball loses the opportunity to decelerate even after the fault is cleared, which indicates that DLP$_3$ would never occur in this case. Further, IMKE$_3$ would keep increasing, and thus, the minimum IMKE$_3$ would never occur during the postfault period, as shown in Fig. 34.

From the analysis above, the reason for the occurrence of the "eternal-accelerating" characteristic of the machine is that the fault-on period lasts too long. Under this circumstance, the fault clearing point (P4) would occur later than the IMPP$_3$ (P3), causing the deceleration area to disappear in the Kimbark curve of the machine.

### B. REPEATED APPEARANCE OF DLPs

Figs. 13 and 14 show that the zero-$f_i$ angle surface of each machine occurs repeatedly on the angle space with the same shape. In this section, this distinctive phenomena is explained in a tutorial using TS-4 as the test bed. A demonstration of the repeated appearance of the zero-$f_2$ surface is shown in Fig. 35.

In Fig. 35, the axis of point A is ($\theta_2$, $\theta_3$), and it satisfies $f_2(\boldsymbol{\theta})$ equal to zero. Point A lies in the zero-$f_2$ surface. Assume point A moves one step ($\theta_2^{mov}$ and $\theta_3^{mov}$). The movement of the point is depicted as

$$\begin{cases} \theta_1^{mov} - \theta_2^{mov} = 2m\pi \quad m = [\ldots -1, 0, 1 \ldots.] \\ \theta_1^{mov} - \theta_3^{mov} = 2n\pi \quad n = [\ldots -1, 0, 1 \ldots.] \\ M_1\theta_1^{mov} + M_2\theta_2^{mov} + M_3\theta_3^{mov} = 0 \end{cases} \tag{15}$$

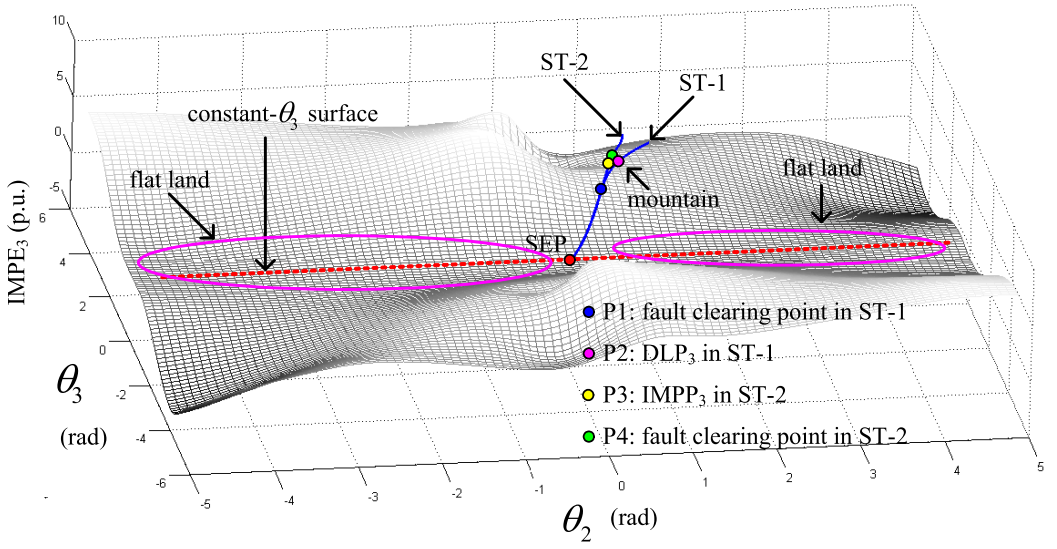


**FIGURE 32.** IMPES of Machine 3.

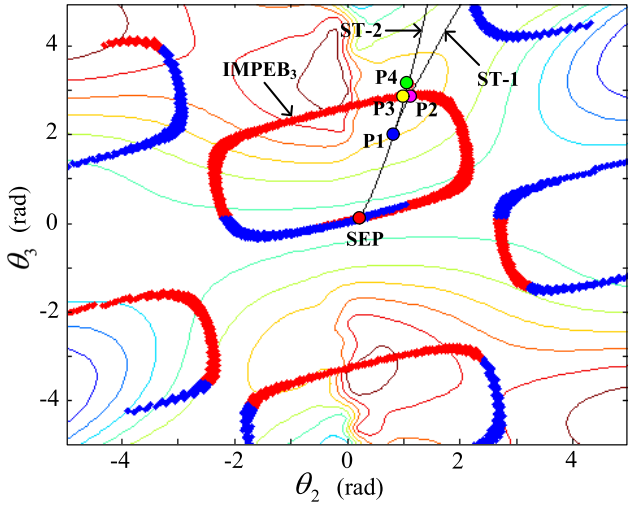


**FIGURE 33.** IMPEB of Machine 3.

Eq. (15) is further denoted as

$$\begin{cases} \theta_2^{mov} = \dfrac{-(M_1+M_3)(2m\pi)+M_3(2n\pi)}{M_T} \\ \theta_3^{mov} = \dfrac{M_2(2m\pi)-(M_1+M_2)(2n\pi)}{M_T} \\ \theta_1^{mov} = \dfrac{M_2(2m\pi)+M_3(2n\pi)}{M_T} \end{cases} \tag{16}$$

After the movement, point A would reach point B. The location of the new point is denoted as

$$\begin{cases} \theta_1' = \theta_1 + \theta_1^{mov} \\ \theta_2' = \theta_2 + \theta_2^{mov} \\ \theta_3' = \theta_3 + \theta_3^{mov} \end{cases} \tag{17}$$

From Eq. (17), using $\boldsymbol{\theta}^{mov}$ as defined in Eq. (16), it is clear that point B also satisfies $f_2(\boldsymbol{\theta}')$ equal to zero. This also indicates that point B lies in another zero-$f_2$ surface

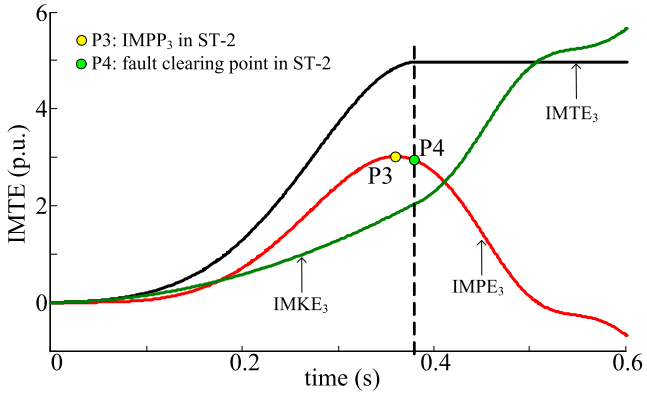


**FIGURE 34.** Variance of IMPE$_3$ along ST-2.

**TABLE 1.** Computed movements.

| $[m, n]$ | $\theta_2^{mov}$ (rad) | $\theta_3^{mov}$ (rad) |
|---|---|---|
| [1,0] | -5.07 | 1.22 |
| [-1,0] | 5.07 | -1.22 |
| [0,1] | 0.57 | -5.71 |
| [0, -1] | -0.57 | 5.71 |

The movements with different combinations of $m$ and $n$ are shown in Table 1.

Using the computed movements as in Table 1, a zero-$f_2$ surface would be formed repeatedly along four directions, as in Fig. 35. Note that IMPE$_2$ at Point B is different from that at Point A.

The repeated appearance of the zero-$f_i$ surface indicates that IMPEB$_i$ would also occur repeatedly. This finding leads to the following two questions:

(i) What is the shape of the Kimbark curve of an unstable critical machine once the system trajectory goes far away from where the first DLP to occur? and (ii) How can this phenomena be explained from the perspective of IMPEB?

Case-3 [TS-4, bus-1, 0.40 s] is used to answer the two questions. The system trajectory [TS-4, bus-1, 0.40 s] is

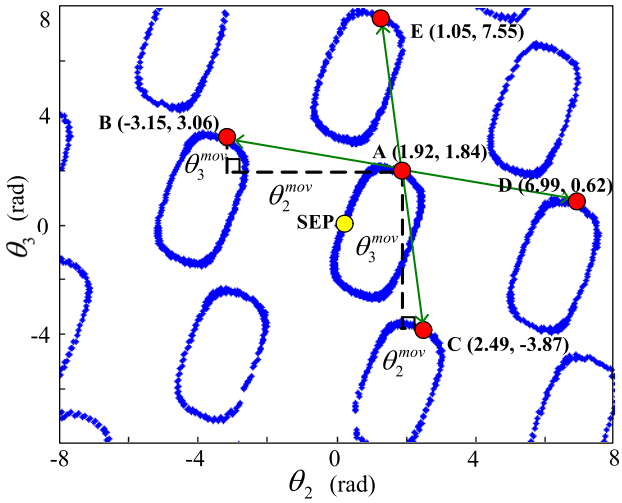


**FIGURE 35.** Repeated occurrence of the zero-$f_2$ angle surface.

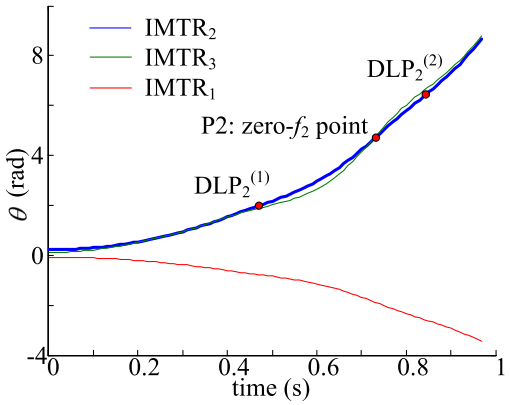


**FIGURE 36.** System trajectory [TS-4, bus-1, 0.40 s].

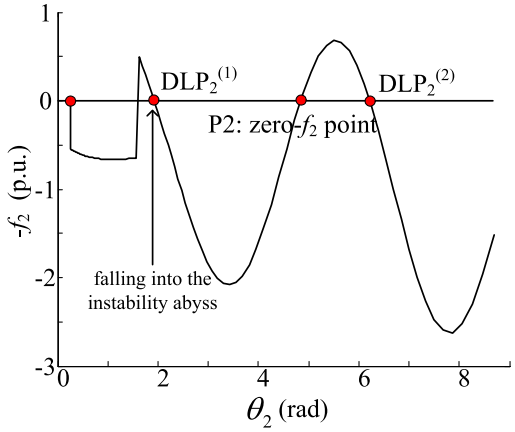


**FIGURE 37.** Kimbark curve of Machine 2 when the system trajectory goes far.

shown in Fig. 36. The Kimbark curve of Machine 2 is shown in Fig. 37. The variance of $IMPE_2$ along the time horizon is shown in Fig. 38. We only focus on the transient behavior of Machine 2 for representation.

As shown in Figs. 36 and 37, from the perspective of IMEAC [8], the Kimbark curve of the machine goes through the zero-$f_2$ horizontal line in $\theta_2$–$f_2$ space repeatedly when the

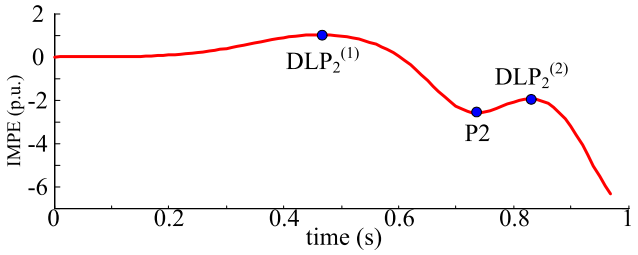


**FIGURE 38.** $IMPE_2$ along time horizon.

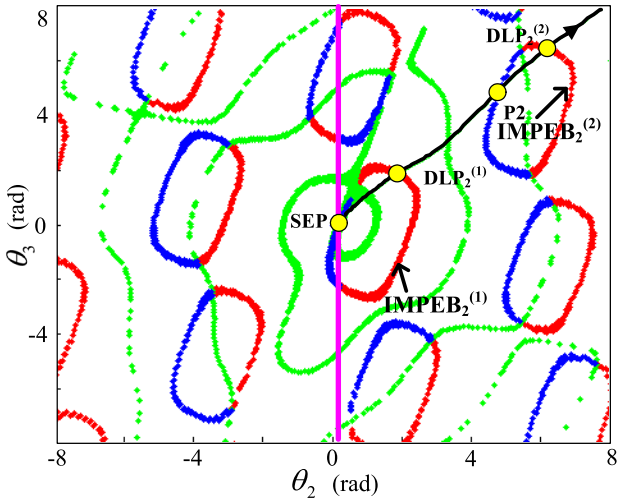


**FIGURE 39.** Appearance of multiple DLPs using $IMPEB_2$.

system trajectory moves forward. $DLP_2^{(1)}$ is the DLP of the machines in the first swing. After that step, Machine 2 starts accelerating until the system trajectory reaches the zero-$f_2$ point (P2). Note that Machine 2 continues to accelerate from $DLP_2^{(1)}$ to P2. Once the system trajectory goes through P2, Machine 2 starts decelerating again until the system trajectory reaches $DLP_2^{(2)}$. From Fig. 38, $IMPE_2$ reaches a maximum at $DLP_2^{(1)}$ and $DLP_2^{(2)}$, and a minimum at P2. The IMPE of the unstable critical machine also shows an "increase-decrease-increase" characteristic along the time horizon.

The phenomena above can be explained visually using the concept of IMPEB. The IMPEB of Machine 2 is shown in Fig. 39, and in this study, we use the same color denotation as that used in Fig. 14.

From Fig. 39, in angle space, the ball first climbs a "mountain", and $IMPE_2$ keeps increasing. At 0.47 s, the ball goes through $IMPEB_2^{(1)}$ at $DLP_2^{(1)}$, and the machine becomes unstable in the first swing. After that step, the ball falls into the instability abyss of the machine. Under this circumstance, Machine 2 accelerates, and $IMPE_2$ keeps decreasing until the system trajectory reaches P2 at 0.74 s. Later, the ball starts to climb another "mountain" until it goes through $IMPEB_2^{(2)}$ at 0.83 s, and the intersection point is $DLP_2^{(2)}$. Note that the energy ball climbs to the "highest" altitude when it goes through $IMPEB_2^{(1)}$ at $DLP_2^{(1)}$ during the entire postfault period, although $IMPE_2$ reaches another "maximum" at a far-away $IMPEB_2^{(2)}$.

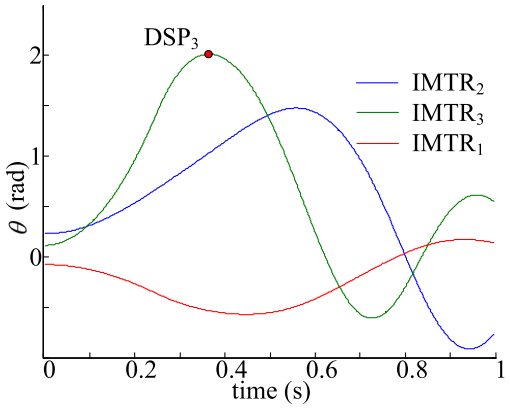


**FIGURE 40.** System trajectory [TS-4, bus-9, 0.250 s].

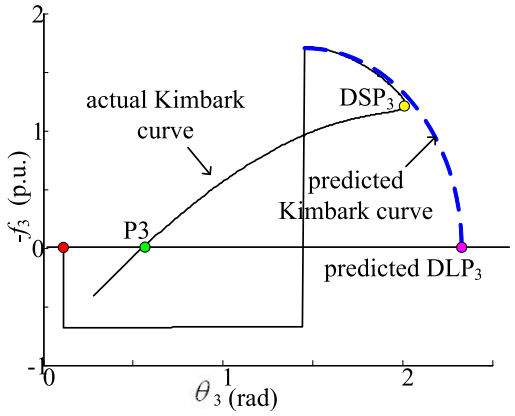


**FIGURE 41.** Kimbark curve of Machine 3.

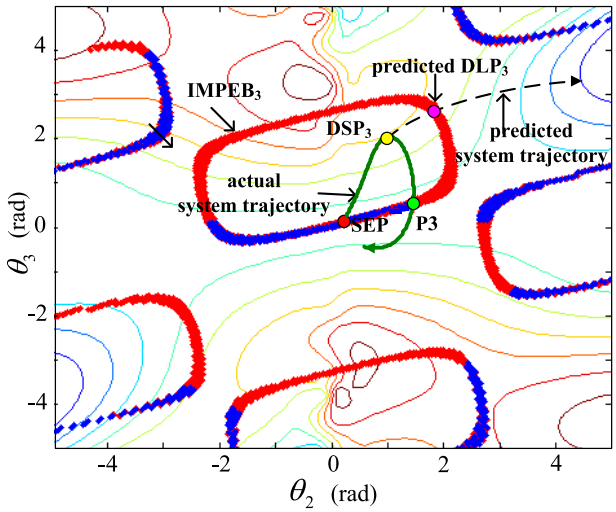


**FIGURE 42.** IMPEB of Machine 3.

From the analysis above, with the energy ball going far away from SEP, the ball may experience a ''climb-fall-climb'' process in the IMPES, which strongly correlates to the ''decelerating-accelerating-decelerating'' process as in the Kimbark curve of the machine.

### C. PHYSICAL NATURE OF THE KIMBARK-CURVE PREDICTION

In global transient energy methods, the sustained fault trajectory in the sustained-fault method [1], [2] and the linear system trajectory in the RUEP method [3] are fictional system trajectories, and they are used to ''approximate'' or ''predict'' the actual system trajectory. Following this fictional system trajectory, the system engineer may observe whether the ''mountain'' in front of the energy ball is high enough to stop it in the PES. Briefly, the fictional system trajectory can be seen as the key concept in transient energy methods because the computation of the exit point and the critical transient energy are fully based on it.

Compared with transient energy methods, the IMEAC method is a genuine EAC method [8]–[10] because it utilizes a predicted Kimbark curve to obtain the DLP of the machine and the corresponding deceleration area. At first glance, it seems that the mechanism of the IMEAC method and that of the transient energy methods are entirely different. However, we emphasize that the IMEAC method is also a trajectory-fiction-based method, and this can be explained using the concept of the IMPEB.

The system trajectory is shown in Fig. 40. The predicted Kimbark curve of Machine 3 is shown in Fig. 41. The IMPEB of Machine 3 is shown in Fig. 42. All machines are stable in this case. We only focus on the transient behavior of Machine 3 for representation.

As shown in Fig. 40, the actual Kimbark curve of Machine 3 inflects back at $DSP_3$ along the actual system trajectory. Note that $DSP_3$ is a 3-dimensional angle vector because it lies in the actual system trajectory, although only the actual $\theta_3$ can be observed in the Kimbark curve. Using the predicted Kimbark curve, the predicted $DLP_3$ ($\theta_3^{pred} = 2.32$ rad) is also obtained.

We explain the process above from the perspective of fictional trajectory. In the $IMPES_3$, the predicted $DLP_3$ satisfies

$$f_3(\theta_1^{pred}, \theta_2^{pred}, \theta_3^{pred}) = 0 \tag{18}$$

In Eq. (18), $\theta_3^{pred}$ is already pre-given from the prediction of the Kimbark curve. The other two angles are obtained as follows

$$M_1\theta_1^{pred} + M_2\theta_2^{pred} + M_3\theta_3^{pred} = 0 \tag{19}$$

From the equations above, the predicted $DLP_3$ strictly lies in $IMPEB_3$ because $f_3$ is zero at this point. Therefore, it is certain that a fictional system trajectory exists between SEP and the predicted $DLP_3$ in $IMPES_3$, as shown in Fig. 42. This fictional system trajectory can be seen as the ''extension'' of the actual stable system trajectory because it goes through $IMPEB_3$ at the predicted $DLP_3$, rather than the actual trajectory that inflects back at $DSP_3$. Therefore, this fictional system trajectory directly correlates to the predicted Kimbark curve of Machine 3.

From the analysis above, similar to the conventional transient energy method, the IMEAC method is also a

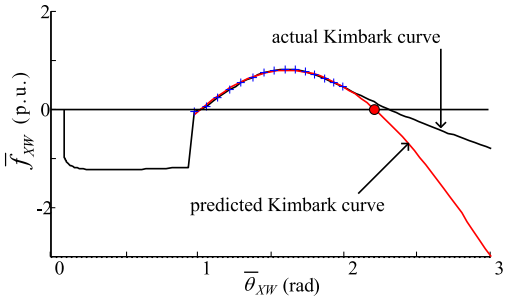


**FIGURE 43.** Predicted Kimbark curve of Gen. #XW [10].

trajectory-fiction-based method. Therefore, one can conclude the following:

*The prediction of the Kimbark curve of an individual machine is identical to the fiction of the system trajectory.*

However, unlike the sustained-fault system trajectory or linear system trajectory that is made in a direct and visualized manner, the fictional system trajectory in the IMEAC method is obtained ''indirectly''. In other words, the fictional system trajectory is obtained through the prediction of the Kimbark curve of an individual machine. This approach is essentially a ''dimensionality reduction'' because the $n$-dimensional multimachine system trajectory is re-described in the two-dimensional $\theta_i$-$f_i$ space. For a multimachine system, each critical machine corresponds to its unique fictional system trajectory through the prediction of its unique Kimbark curve (the fictional system trajectory corresponding with each machine is different). Each fictional system trajectory is only used to evaluate the stability state of the corresponding critical machine along it. This can be seen as the fundamental mechanism of the IMEAC method.

This advantage is nicely demonstrated when using the reference-machine-based IMEAC method (RM-IMEAC) in TSA [10]. Using TS-3 as the test bed, the fault is set as [TS-3, line-LIAOC_TANZ, 0.22 s]. In this case, the reference machine is selected as Gen. #LZ in SYSTEM_SD. The predicted Kimbark curve is shown in Fig. 43. Note that the reference in the following analysis is set as the RM rather than the COI-SYS.

In Fig. 43, the Kimbark curve of Gen. #XW in the RM reference is predicted through the parameters of only two real machines in the system, i.e., Gen. #XW and Gen. #LZ. However, such a prediction of the Kimbark curve is completely identical to the fiction of the entire 146-machine system trajectory. Along this fictional system trajectory, Gen. #XW (in the RM reference) becomes unstable at the predicted DLP, i.e., the intersection point between the fictional system trajectory and $\text{IMPEB}_{\#XW}$.

From the analysis above, the prediction of the 146-machine system trajectory can be obtained in an indirect manner by using the parameters of only two physical real machines in the system. This visually shows the distinctive advantage of the RM-IMEAC method in TSA [10].

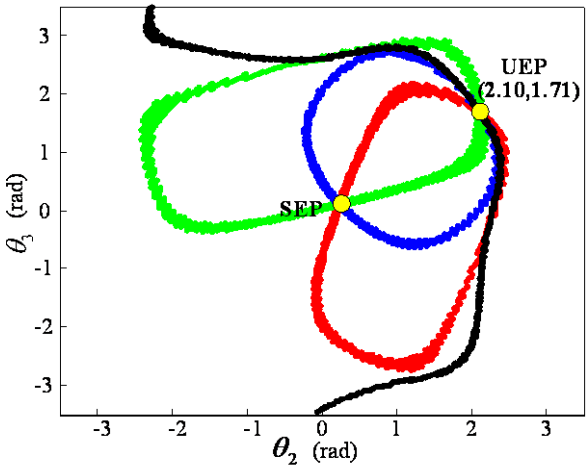


**FIGURE 44.** Formation of UEP using zero-$f_i$ angle surface.

### D. RE-EXPLANATION OF UEP BY USING IMPES

In global transient energy methods, UEP is used as the approximation of the critical energy point of the system; thus, it is a key concept in global transient energy. In this section, this concept can be re-explained using the concept of a zero-$f_i$ angle surface as defined in Section IV A.

The UEP and SEP are denoted as

$$f_i(\boldsymbol{\theta}) = 0 \quad i = 1, 2 \cdots n \tag{20}$$

From Eq. (20) and the definition of the zero-$f_i$ angle surface as in Eq. (10), it is quite clear that the UEP can also be depicted as the ''intersection point'' of the zero-$f_i$ angle surfaces of all machines in the system. For example, for the TS-1 with ten machines, the UEP should be mathematically depicted as the intersection point of the zero-$f_i$ angle surfaces of all the ten machines in the system, because each zero-$f_i$ angle surface goes through UEP.

Demonstration of UEP using a small test bed TS-4 is shown in Fig. 44. From the figure, it can be found that only one UEP physically exists in this three-machine system.

The individual-machine-based analysis of UEP is of value because it reveals that the UEP method might fail in certain simulation cases. In particular, the combinations of mode of disturbances (MOD) in this case should be $2^{n-1}$-1 types (three MODs), and they directly correspond to $2^{n-1}$-1 UEPs (three UEPs) that theoretically exist. However, from this case study, it is found that only one UEP physically exists (this UEP corresponds to the MOD that both Machines 2 and 3 become unstable), while the other two UEPs do *not* exist, as in Fig. 44. Under this circumstance, all the three possible MODs in this simulation case are forced to correlate to this ''one and only'' physical UEP. For instance, the MOD in Fig. 1 (b) is described as Machine 2 being a non-critical machine while Machine 3 becoming unstable. However, this MOD *cannot* find its correlated UEP. In fact, the absence of UEPs may also explain why some ''theoretical'' UEPs *cannot* be obtained after hundreds of iterations in certain simulation cases [12], because they ''physically'' do not exist.

## VII. CONCLUSION

This paper proposed the concept of IMPES for the first time in the history of individual-machine-based transient stability studies. It is found that a constant-$\theta_i$ angle surface exists in the IMPES. The IMPE of Machine $i$ in the constant-$\theta_i$ angle surface is strictly zero. The IMPES is separated by a ''flat land'' with very low IMPE. Mountains and valleys are located on either side of this flat land in each IMPES. Using the definitions of the scissor angle surface, the IMPEB is obtained through the cut of the zero-$f_i$ angle surface. Distinctive phenomena such as multiswing instability and the eternal-accelerating Kimbark curve can be explained using IMPES. It shows that the repeated appearance of DLPs of an unstable critical machine can be explained using the repeated appearance of the IMPEB in the angle space. It is proven that the IMEAC method is also a fictional-system-trajectory-based method that uses the prediction of the Kimbark curve of the machine. In the end, the concept of UEP is re-explained using the zero-$f_i$ angle surface. In this way the inherent defect of the UEP is fully exposed through individual-machine perspective. The IMPES proposed in this paper theoretically validates the effectiveness of the IMEAC method.

In the following paper, the mechanism of the transient energy conversion inside an individual machine will be systematically explained by using genuine Newtonian mechanics. Revealing the nature of the individual-machine transient stability through Newtonian physics may enable the further elucidation of the power system transient stability for both researchers and industrial practitioners.

## REFERENCES

[1] N. Kakimoto, Y. Ohsawa, and M. Hayashi, ''Transient stability analysis of electric power system via Lur's type Lyapunov function, Part I new critical value for transient stability,'' *IEE Trans. Jpn.*, vol. 98, nos. 5–6, pp. 63–71, 1978.

[2] N. Kakimoto, Y. Ohsawa, and M. Hayashi, ''Transient stability analysis of electric power system via Lur's type Lyapunov function, Part II modification of Lure type Liapunov function with effect of transfer conductances,'' *IEE Trans. Jpn.*, vol. 98, nos. 5–6, pp. 72–79, 1978.

[3] T. Athay, R. Podmore, and S. Virmani, ''A practical method for the direct analysis of transient stability,'' *IEEE Trans. Power App. Syst.*, vol. PAS-98, no. 2, pp. 573–584, Mar. 1979.

[4] V. Vittal, ''Power system transient stability using critical energy of individual machines,'' Ph.D dissertation, Dept. Elect. Eng., Iowa State Univ., Ames, IA, USA, 1982.

[5] A. Michel, A. Fouad, and V. Vittal, ''Power system transient stability using individual machine energy functions,'' *IEEE Trans. Circuits Syst.*, vol. CAS-30, no. 5, pp. 266–276, May 1983.

[6] S. E. Stanton, ''Transient stability monitoring for electric power systems using a partial energy function,'' *IEEE Trans. Power Syst.*, vol. 4, no. 4, pp. 1389–1396, Nov. 1989.

[7] R. Ando and S. Iwamoto, ''Highly reliable transient stability solution method using energy function,'' *IEE Trans. Jpn.*, vol. 108, no. 4, pp. 253–260, Jun. 1988.

[8] S. Wang, J. Yu, and W. Zhang, ''Transient stability assessment using individual machine equal area criterion PART I: Unity principle,'' *IEEE Access*, vol. 6, pp. 77065–77076, 2018.

[9] S. Wang, J. Yu, and W. Zhang, ''Transient stability assessment using individual machine equal area criterion PART II: Stability margin,'' *IEEE Access*, vol. 6, pp. 38693–38705, 2018.

[10] S. Wang, J. Yu, and W. Zhang, ''Transient stability assessment using individual machine equal area criterion PART III: Reference machine,'' *IEEE Access*, vol. 7, pp. 80174–80193, 2019.

[11] S. Wang, J. Yu, A. M. Foley, and W. Zhang, ''Transient energy of an individual machine PART I: Stability characterization,'' *IEEE Access*, vol. 9, pp. 44797–44811, 2021.

[12] A. Fouad, V. Vittal, and T. Oh, ''Critical energy for direct transient stability assessment of a multimachine power system,'' *IEEE Trans. Power App. Syst.*, vol. PAS-103, no. 8, pp. 2199–2206, Aug. 1984.

**SONGYAN WANG** received the B.S., M.S., and Ph.D. degrees from the School of Electrical Engineering and Automation, Harbin Institute of Technology (HIT), in 2007, 2009, and 2012, respectively. He was a Visiting Scholar with Virginia Tech, VA, USA, in 2010. From 2013 to 2014, he was a Research Fellow with Queen's University Belfast, U.K. He is currently an Assistant Professor with HIT. His research interests include power system operation and control. He is an Associate Editor of *Renewable and Sustainable Energy Reviews*.

**JILAI YU** joined the School of Electrical Engineering and Automation, Harbin Institute of Technology, in 1992. From 1994 to 1998, he was an Associate Professor with the School of Electrical Engineering and Automation, where he is currently a Professor and the Director of the Electric Power Research Institute. His current research interests include power system analysis and control, optimal dispatch of power systems, green power, and smart grids.

**AOIFE M. FOLEY** (Senior Member, IEEE) received the B.E. degree in civil engineering from Irish Power System, University College Cork, Ireland, in 1996, the M.Sc. degree in transportation engineering from Trinity College Dublin, University of Dublin, Ireland, in 1999, and the Ph.D. degree in unit commitment modeling of wind and energy storage from Irish Power System, University College Cork, in 2011. She worked in industry for 12 years for ESB International, Siemens, SWS Energy, and PM Group, mostly in the planning, design, and project management of energy, telecoms, waste, and pharma projects. She is currently a Reader with the School of Mechanical and Aerospace Engineering, Queen's University Belfast, U.K. Her research interests include energy system modeling focused on electricity systems, markets and services, wind power, electric vehicles, and smart technologies. She was a Founding Member of the IEEE VTS, U.K., and the Ireland Chapter, in 2011. She is a Chartered Engineer, in 2001, a Fellow of the Engineers Ireland, in 2012, and a member of the IEEE PES and IEEE VTS. She is also the Editor-in-Chief of *Renewable and Sustainable Energy Reviews*.

**WEI ZHANG** (Senior Member, IEEE) received the B.S. and M.S. degrees in power system engineering from the Harbin Institute of Technology, Harbin, China, in 2007 and 2009, respectively, and the Ph.D. degree in electrical engineering from New Mexico State University, Las Cruces, NM, USA, in 2013.

He is currently an Associate Professor with the School of Electrical Engineering and Automation, Harbin Institute of Technology. His research interests include distributed control and optimization of power systems, renewable energy and power system state estimation, and stability analysis.